GOETHE UNIVERSITÄT FRANKFURT AM MAIN

Master Thesis in Geophysics, August 2015

Thermal, electrical and elastic properties of the Moon

- a multi-physical joint inversion -

NAWA, VIKTOR

Supervisor:

Apl. Prof. Nikolai Bagdassarov

Co-corrector:

Prof. Dr. Harro Schmeling

Abstract

This master study deals with constrains of mineralogical and thermal structure of the moon based on the analysis of Love-number and magneto-electric observations on the lunar surface. Therefore the thermal evolution of the moon beginning from the moment of the complete differentiation till today has been modeled using a 1D finite difference code. For the thermal evolution model the parameters of thermal conductivity, heat capacity and density were taken as temperature and partly pressure dependent, resulting in a time-dependence of these properties. Furthermore, the convection inside the moon has been implemented using an effective thermal conductivity based on Nusselt number. Melting processes and the related latent heat of iron and silicate melting were taken into account using an effective heat capacity. The radiogenic heat production has been modelled including a fractionation of incompatible radioactive elements into a temporally growing crust. The derived selenotherm has then been used to model the elastic deformation response due to the Earth-Moon-tides in a form of the k_2 Love number and the tidal dissipation factor Q. The electrical conductivity of the lunar rocks were evaluated from the temperature profile in order to calculate the lunar day side magnetometer transfer function. Furthermore, additional electrical conductivtity measurements of lunar analogue materials have been carried out. The modelled results were compared with the observed lunar mass, moment of inertia, k_2 Love number and magnetometer transfer-function. The parameters of mineralogical boundaries between crust/upper-mantle, upper/lower mantle and core/mantle, the lunar minerals water content and the initial temperature after differentiation were chosen by applying a fitting procedure using a Downhill Simplex algorithm. The obtained results imply that the lunar near side crust has a thickness of 40 ±3 km, the inter-mantle boundary lies in a depth of 930 ±14 km below the surface and the radius of the core is 475 ±9 km. Further the initial temperature after differentiation is found to be 2910 ±40 K. The amount of water in the lunar minerals is about 15 ±3 ppm.

Contents

65

0 Abstract 2

Contents 3

1 Introduction

1.1 Aim of this thesis 5

1.2 State of research 6

2 Model Description

2.1 Mineralogical constraints 7

2.2 Thermal evolution model

2.2.1 Heat equation 10

2.2.2 Thermal conductivity and effective thermal conductivity 11

2.2.3 Heat capacity and effective heat capacity 13

2.2.4 Density and elastic moduli 15

2.2.5 Lunar mass, moment of inertia and pressure 17

2.2.6 Heat production 19

2.2.6 Numerical discretization of the thermal evolution model 20

2.3 Tidal deformation

2.3.1 Tidal forces 22

2.3.2 Tidal deformation and Love numbers 24

2.4 Electrical conductivity

2.4.1 Electrical conductivity of rocks and minerals 26

2.4.2 Electrical conductivity measurements of lunar analogue materials 28

2.4.3 Magnetometer measurements 31

2.4.4 Numerical discretization of the electrical conductivity model 34

2.5 Inversion strategy

2.5.1 Downhill Simplex algorithm 35

2.5.2 Observed data and parameters 38

2.5.3 Misfit calculation and weighting 40

2.6 Definition of variables and parameters 42

3 Inversion Results 44

4 Discussion

4.1 Comparision to other results 52

4.2 Simplifications and neglected aspects 54

5 Outlook 55

6 Acknowledgements 55

7 Bibliography 56

Appendix A – Numerical codes 59

Appendix B – Parameter values 75

1 Introduction

The aim of this chapter is to present the current state of research and a brief history of the lunar thermal evolution.

1.1 The aim of this thesis

The aim of this master thesis is to find an answer on the five following questions:

1. Does the Moon have a molten core?
2. Does the Moon have a partially molten lower mantle?
3. Which size does the lunar core, the upper and lower mantle and the crust have?
4. What water content can be expected for lunar minerals?
5. What were the initial temperature conditions during the formation of the Moon?

In order to resolve these five issues an numerical model of inversion strategy was develloped. The derived model consists of three submodels. First of all, the thermal evolution process of the moon is simulated from the moment of the Moons diffrentiation till now. The derived temperature distribution is then used for modelling an electrical conductivity and an elastic moduli profile. The conductivity profile is used in the second submodel to derive the magnetometer transfer function. The elastic property profile is used to calculate the lunar deformation under the influence of the Earth-Moon tides. The electrical and elastic properties are not solely dependent on the temperature distribution and the mineralogical structure but also on the water content in lunar minerals.

The motivation behind this thesis is to clarify the above mentioned questions regarding the contradicting results of previous works. The main contradictions are formulated in the next paragraph.

1.2 Current state of research

The first noteworthy presentations of the lunar interior structure were published in the late 1960s in the context of NASAs Apollo program. With the availability of lunar magnetometer measurements, the focus was on linking the electrical conductivity profile to the selenotherm. Furthermore, seismological research have been carried out based on the lunar seismometer recordings. *Duba and Ringwood (1972)* presented the interpretation of the magnetometer observations by assuming a lunar mantle composition dominated by ortho-pyroxene. They have compared the temperature dependent conductivity of this mineral with the electrical conductivity structure obtained by magnetometers. As a result they could estimate the interior temperature of the moon slightly below the solidus temperature (~1300 K) in 500 to 900 km depth. Furthermore, the existence of a metallic core has been suggested due to the high electrical conductivity in deep regions. *Olhoeft et al (1973)* discussed the difficulties of electrical conductivity measurements of lunar materials with respect to the oxygen fugacity fO_2. The mineral conductivities under strongly reducing conditions on the Moon can not therefore be described by the measurements under terrestial conditions. *Leavy et al (1974)* derived a conductivity model of the Moon from magnetometer data and postulated a practically water free lunar mineralogy judging from electrical conductivity of pyroxenes at high temperature. *Fisher et al (1977)* carried out some new conductivity measurements on lunar samples returned from the Apollo missions under low oxygen fugacity conditions and derived a selenotherm ranging up to 1500 K in the centre of the moon. *Hobbs et al (1983)* used the electrical conductivity profile derived from the magnetometer data to give an upper boundary for the lunar core radius. The result of this work indicates a maximum radius of 435 km. *Khan et al (2006)* derived a numerical model to calculate the tidal deformation of the Moon. They have choosen the best possible model by variying certain parameters using a Monte Carlo inversion algorithm. As a result they have found out that the lunar core is molten and it is about 350 km in size. However, their results are equivocal, because the

presence of a molten envelope around the core may decouple it mechanically from the surrounding mantle. The existence of a viscous layer in a form of molten iron or partially molten lunar mantle surrounding the solid iron core could provide the same effect on Love numbers. With ongoing research using recent data of the k_2 Love-numer the existence of a lunar core has been suggested, the question of the state of the core still remains open. *Khan et al (2004)* used the lunar tidal deformation measured by the lunar laser ranging method and the lunar prospector probe to give constraits on the size and the state of the lunar core. *Khan et al (2014)* carried out an inversion similar to the previous study, taking into account the more recent satellite measurements of the k_2 Love-number, lunar mass, moment of inertia (all from *Williams et al (2014)*) and magnetometer transfer-function (from *Hobbs et al (1983)*). Their aim was to find out whether a deep layer with partial melt does exist on the lunar core-mantle boundary. As a result they proposed a ~200 km thick layer with partial melting at the depth between 1200 and 1400 km surrounding the Moons core. The existance of a deep partially molten layer inside the Moon has been already postulated in a short treatise of *Williams et al (2002)*. These authors compared seismic velocities derived from the Apollo missions seismometers and found a strong attenuation of seismic waves in the above mentioned depths. In the work of *Garcia et al (2014)* a preliminary lunar reference model is presented which is based on the inversion of seismic velocities obtained from the Apollo seismometer recordings and the additional geodesic observations. They assumed a homogenous mantle and did not consider possible melt zones in the mantle. Their model indicates a core size of about 380 km with a liquid outer core and a density of 5200 kg/m³. Finally, the research carried out in the last 40 years could provide some constraints of the lunar interior, but yet there are some open questions and contradicting results. The derived selenotherms of different authors are quite differing, the question whether the core is solid or molten is not finally resolved, and the content of lunar water in rocks is assumed to be low, but this has not yet been implemented in the numerical models of lunar thermal evolution, in profiles of the electrical conductivity with depth and in lunar tidal dissipation models.

2.1 Mineralogical Constraints

For the modeling of the thermal evolution, the tidal-elastic behaviour and the electrical conductivity depth profile of the moon, the most plausible mineralogical composition is usually used. Generally, the Moon is segmented in a anorthositic/basaltic crust, in a pyroxene-olivine mantle and in an iron alloy core. But throughout the existing literature on the lunar structure there are two prevalent ideas how the lunar interior may be composed. The difference between the two concepts is whether the lunar mantle is uniform or it is divided in an upper and a lower part regarding to the mineralogical composition. The lunar mantle subdivision from the model of *Kuskov et al (2014)* was applied in this study. In the work of *Kuskov et al (2014)* the inversion of seismic velocities was carried out, using a thermodynamic mineral phase equilibrium model for the system of Na_2O–TiO_2–CaO–FeO–MgO–Al_2O_3–SiO_2. Seismic velocities has been estimated from an averaging procedure of individual mineral phases at respective pressure and temperature. The results of their inversion are as follows: The lunar mantle is divided into a lower and an upper section with differing mineralogical and chemical compositions. For the upper mantle the major phase is ortho-pyroxenes (~76 %) with minor fractions of olivin (11-14 %), clino-pyroxene (~9 %), titanite (0.45 %) and spinell/garnet (1-2 %). The lower mantle was determined to consist of olivine (54 %) and clino-pyroxene (37-40 %) as dominant phases with minor amounts of garnet (4-5 %), ortho-pyroxene (0-4 %) and

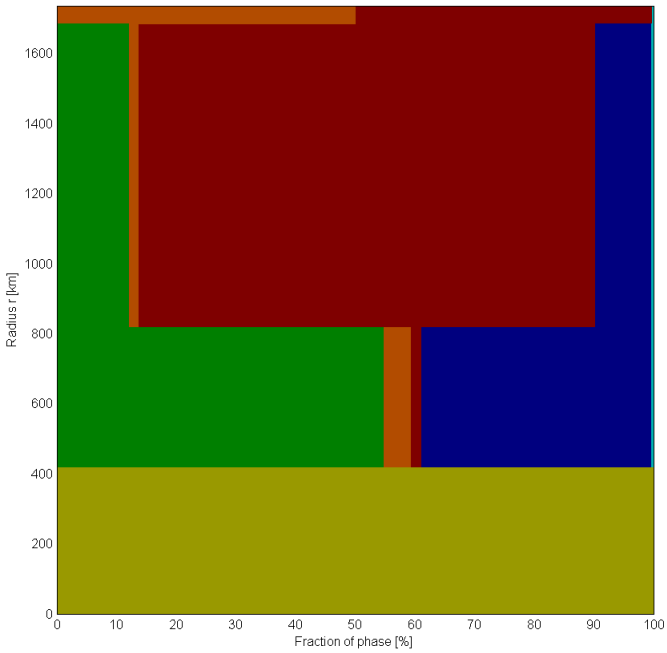

Figure 1: Mineralogical composition for the inversion: ■ Olivine, ■ Al-phase (Feldspar, Spinel, Garnet), ■ Ortho-Pyroxene, ■ Clino-Pyroxene, ■ Titanite, ■ Iron-nickel-alloy

titanite (0.4 %) (Fig. 1).

The composition of the upper lunar crust is well determined thanks to the collected samples of NASA's Apollo and soviet Luna space missions. The brighter regions of the surface consisting of the anorthositic material, while the large, dark plains (so called maria) are of the basaltic origin. To account for both, the crustal composition was assumed to be an anorthite rich basalt composed of 50 % anorthite and 50 % ortho-pyroxene. The lower parts of the crust are assumed to consist of a so called KREEP-layer. The term KREEP stands for potassium (K), rare-earth-elements and phosphorus. This came from the hypothesize that the lunar magma ocean after the lunar accretion and differentiation stages has been enriched in these incompatible elements and ascended due to the lower density upwards to the surface, crystallized and formed a layer on the present upper mantle-crust boundary. The still more lighter anorthitic feldspars have been floaten up during this process, reaching the surface and forming the upper crust. Later, in some areas of the Moons crust some sporadic volcanic processes and impacts carried the KREEP-material to the surface, for example in the Mare Procellarum or the Montes Apenninus region. From both these sites the samples were collected and returned to the Earth during NASAs Apollo mission. Analysis of these samples gave a direct evidence for the existence of the mineralogical feature of the KREEP-material. For the thermal evolution model the KREEP layer won't be taken into account, as it is assumed that the material behaves like pyroxenite regarding to its thermal properties (thermal conductivity, heat capacity and density) (*Grimm (2013)*).

The lunar core composition still remains uncertain. While the main component is an iron-nickel-alloy, some small amounts up to 10 wt.-% may be lighter elements like sulfur and/or oxygen. In this work the core is assumed to be a pure iron-nickel-alloy neglecting the presence of light elements, even though these components have a large influence on the physical properties like solidus and liquidus temperatures or density of the core material.

2.2 Thermal evolution

The thermal evolution of the moon has been calculated by solving the time dependent heat equation using a 1D finite difference approach. In this chapter the heat equation, boundary conditions and the pressure-temperature dependent thermal properties will be presented together with the numerical discretization scheme.

2.2.1 Heat equation

The heat equation is a partial differential equation that describes the temporal and spatial temperature change in a system over time.

$$\frac{\partial T}{\partial t} + \vec{v} \cdot \nabla T = \frac{1}{\rho \cdot c_P} \cdot \nabla (\lambda \cdot \nabla T) + \frac{H}{c_P} \quad (1)$$

The first term on the left side describes the temporal change in temperature, the second term is the advection of heat, the first term on the right side is related to the the spatial temperature change and the second one to the production of heat inside the system. However, this equation will be modified to avoid the calculation of the convection velocity field $\vec{v}$. The following paragraphs describe the modifications of the equation and the dependencies of the containing parameters.

2.2.2 Thermal conductivity and effective thermal conductivity

The transfer of heat in materials can be split up in two components: conduction and advection of heat. The conduction of heat takes place on one hand due to thermal oscillations of atoms and on the other hand by thermal radiation. The thermal conductivity λ quantifies both of these processes. The first term on the right hand side of Eq. 1 accounts for this. The advection of heat takes place in liquid media, however, also solid materials can be treated as liquids when they show a viscous behavour. In the case of heat transfer in a system with hot temperature at the bottom and cold temperature at the top, like in the interior of many celestial bodies, thermal density variations creating buoyancy, forcing the hot material to rise upwards and cold material to sink downwards due to the thermal expansivity and density changes. This process is called convection and it can outnumber the amount of heat transported by conduction by several orders of magnitude. For the process of the heat advection, the velocity field $\bar{v}$ in Eq. 1 has to be computed by the Navier-Stokes-Equation. To quantify the amount transported by advection without fluid-dynamic modelling, a Nusselt-Number/Rayleigh-Number (Nu/Ra) relation can be applied, replacing the thermal conductivity by an effective thermal conductivity in Eq. 1. The dimensionless Rayleigh-Number (Ra) describes the vigour of convection inside a system. It is defined as:

$$Ra = \frac{g \cdot \alpha \cdot \rho \cdot c_P \cdot \Delta T \cdot h^3}{\lambda \cdot \eta} \quad (2)$$

where g is the gravitation acceleration, α is the thermal expansivity, ρ is the density, c_P is the heat capacity, ΔT is the temperature difference between the upper and the lower boundary of the convecting layer, h is the thickness of the convecting layer, λ is the thermal conductivity and η is the viscosity. The higher the Rayleigh number is, the more intense is the convection process. However,

Ra must exceed a critical Rayleigh number Ra_c so that convection starts to take place. In the case of convection in a spherical shell the critical Rayleigh-Number Ra_c = 1296 with no-slip boundary conditions at the surface and the bottom (*Iwase and Honda (1997)*).

The dimensionless Nusselt-number (Nu) describes the amount of total transferred heat compared to a pure conductive heat without advection. The Nusselt number is given by

$$Nu = \frac{q_{top} \cdot h}{\lambda \cdot \Delta T} \quad (3)$$

where q_{top} is the heat flow on the upper boundary of the convective layer. Nu is always equal or greater 1.

The relation between Nu and Ra can be obtained from the numerical modellation of convection processes at different values of Ra. Typically it results in a scale law of the form:

$$Nu(Ra) = \gamma \cdot Ra^{\beta} \quad (4)$$

The parameters for this relation were adopted from *Iwase and Honda (1997)*. If the Rayleigh-number Ra inside a system is known, an effective thermal conductivity is given by:

$$\lambda_{eff} = \lambda \cdot Nu(Ra) \quad (5)$$

The effective thermal conductivity accounts for the transported heat by conduction and advection. This leads to the heat equation in the form:

$$\frac{\partial T}{\partial t} = \frac{1}{\rho \cdot c_P} \cdot \nabla(\lambda_{eff} \cdot \nabla T) + \frac{H}{c_P} \quad (6)$$

2.2.3 Heat capacity and effective heat capacity

For the lunar crust, the upper and the lower mantle the major mineral phases are olivine and pyroxene. The heat capacity for this part of the moon is composed of the heat capacity of these two phases with respect to their fraction f_i.

$$c_p = \frac{f_{Ol}}{f_{Ol}+f_{Px}} \cdot c_P^{Ol} + \frac{f_{Px}}{f_{Ol}+f_{Px}} \cdot c_P^{Px} \quad (7)$$

The heat capacity of olivine and pyroxene is calculated as a function of temperature (*Watanabe (1982)*). Further it was assumed, that pressure effects can be neglected. The heat capacity for olivine and pyroxene is given by

$$c_P^{Ol/Px} = c_A + c_B \cdot T + c_C \cdot T^{-2} + c_D \cdot T^{-\frac{1}{2}} + c_E \cdot T^2 \quad (8)$$

with different coefficients c_x, respectively. For the lunar core a constant heat capacity of iron was chosen with a value of 700 J/(kg·K) (*Interior Structure of the Earth and Planets, V. N. Zharkov, p. 114*).

Further, the latent heat released by a phase transformation was taken into account in form of an effective thermal capacity. This effective thermal capacity enhances the normal thermal capacity c_P in the temperature range between the solidus and liquidus of a phase. $c_{P\,eff}$ is then given by

$$c_{P\,eff} = c_P + \frac{L}{T_{liq}-T_{sol}} \quad (9)$$

where L is the latent heat of fusion of silicate or iron, T_{liq} and T_{sol} are the liquidus and solidus temperatures, respectively. For the pyroxene-rich upper mantle the Clapeyron-equation for liquidus and solidus were taken from *Smith et al (2003)*. For the lower mantle which is dominated by olivine, solidus and

liquidus were taken from *Thompson et al (2000)*. For the lunar core an iron/nickel alloy has been assumed. The corresponding liquidus and solidus temperatures were adopted from *Ahrens et al (2002)*. The pressure and temperature dependent liquidus and solidus conditions for these phases are shown in Fig. 2.

For the calculation of the melt fraction in different depths, a linear relation between solidus (melt fraction zero) and liquidus (melt fraction 1 = 100%) was assumed.

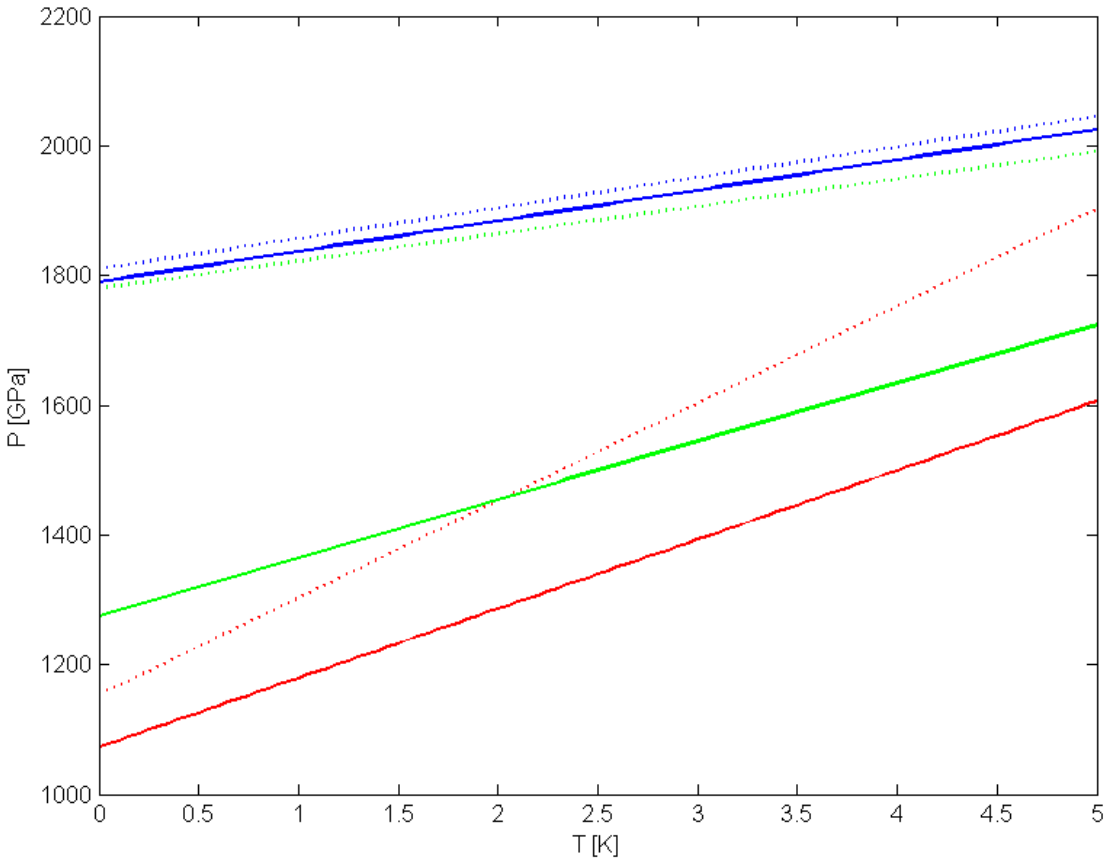

Figure 2: *Solidus (solid lines) and liquidus (dotted lines) for Peridotite ●, Pyroxenite ● and Iron/Nickel ●.*

2.2.4 Density and elastic moduli

The density of a phase is a function of temperature and pressure, and this can be formulated as followed:

$$\rho(P,T) = \rho_0 \cdot \left(1 - \alpha \cdot T + \frac{P}{K}\right) \quad (10)$$

Where ρ_0 denotes a reference density, α is the thermal expansivity and K is the bulk modulus. α and K are both dependent on pressure and temperature, too. For a simplification α will be taken constant, but for the bulk modulus K the derivatives for pressure and temperature are well estimated for a lot of individual minerals thanks to the laboratory researches. The bulk modulus K as a function of pressure and temperature is given by:

$$K(P,T) = K_0 \cdot \left(1 + \frac{\partial K}{\partial T} \cdot T + \frac{\partial K}{\partial P} \cdot P\right) \quad (11)$$

This formulation is also applied by analogy to the shear modulus G. The values for α, K_0, G_0 and the corresponding temperature and pressure derivatives can be found in Table 8 in Appendix B. For the calculation of a mean shear- and mean bulk-modulus of each layer the method of Hashin-Shtrikman-bounds for elastic moduli has been chosen. This averaging method assumes an isotropic and homogenious distribution of individual phases in a rock. Eq. 12 and Eq. 13 for the computation scheme can be found in *The Rock Physics Handbook, Mavko et al (1998)*.

$$\begin{aligned} K^+ &= \Delta(G_{max}) & K^- &= \Delta(G_{min}) \\ G^+ &= \Gamma(\zeta(K_{max}, G_{max})) & G^- &= \Gamma(\zeta(K_{min}, G_{min})) \end{aligned} \quad (12)$$

The index +/- denotes the upper/lower bounds for the elastic moduli. The index min/max refers to the lowest/highest modulus value of the participating

phases. The functions Λ, Γ and ζ are explained in Eq. 13

$$\Delta(z) = \left[\sum_{i=1}^{I} \frac{1}{K_i \cdot f_i + \frac{4}{3} \cdot z}\right]^{-1} - \frac{4}{3} \cdot z$$

$$\Gamma(z) = \left[\sum_{i=1}^{I} \frac{1}{G_i \cdot f_i + z}\right]^{-1} - z \qquad (13)$$

$$\zeta(K, G) = \frac{G}{6} \cdot \left(\frac{9 \cdot K + 8 \cdot G}{K + 2 \cdot G}\right)$$

The resulting upper and lower bounds for the shear-modulus as a function of depth will be later used for the tidal deformation model. Furthermore, the upper and lower bounds for a seimsic velocity profile will be calculated using the following equations:

$$V_P^{+/-} = \sqrt{\frac{K^{+/-} + \frac{4}{3} G^{+/-}}{\rho}} \quad (14)$$

$$V_S^{+/-} = \sqrt{\frac{G^{+/-}}{\rho}} \quad (15)$$

Indices +/- correspond to the upper and lower bounds of the S- and P-Wave velocities and elastic moduli, respectively.

2.2.5 Lunar mass, moment of inertia, gravitation acceleration and pressure

The lunar mass and the moment of inertia are two out of four observed quantities that were chosen for the inversion (the other two are the magnetometer transfer function and the k_2 Love number). The reference values for the lunar mass and moment of inertia have been adopted from *Williams et al (2014)*. The lunar mass m within a radius r' is calculated from Eq. 16.

$$m(r') = \int_0^{r'} 4 \cdot \rho(r) \cdot \pi \cdot r^2 \, dr \quad (16)$$

by integration from the center r=0 to r=r'. Integration of Eq. 16 from the center to the surface gives the lunar mass M (Eq. 17).

$$M = m(r = R) \quad (17)$$

The moment of inertia I is obtained by the integration Eq. 18 from the center to the surface.

$$I = \int_0^{R} 2 \cdot \pi \cdot r^4 \cdot \rho(r) \, dr \quad (18)$$

The non-dimensional moment of inertia is obtained according to Eq. 19.

$$J = \frac{I}{M \cdot R^2} \quad (19)$$

The profile of the gravitation acceleration g(r) is calculated as followed in Eq. 20.

$$g(r) = \frac{G \cdot m(r)}{r^2} \quad (20)$$

The radial pressure profile P(r) is obtained by the integration of Eq. 21 from the surface to the centre.

$$dP = \rho \cdot g \cdot dr \quad (21)$$

2.2.6 Heat production

The heat production inside the moon after the accretion stage mostly stems from the decay of U-238, U-235, Th-232 and K-40. At the time of the formation of the Moon 4.4 Ga ago, it was assumed that the accreted material was chondritic. Further, it was supposed that the core formed very quickly after the accretion, so that the thermal evolution (cooling) model starts with an already fully differentiated body at the temperature above liquidus. With the assumption that the moon consists of the chondritic material, the initial lunar mantle composition was enriched by the amount of U, Th and K which have not been partitioned into the core ($D_{mantle/core}$ = 0). The inital mantle concentration at t=-4 Ga of an isotope X is then given by

$$[X]_{mantle}^{t=-4\,Ga} = [X]_{chondritic}^{t=-4\,Ga} \cdot \frac{M_{total}}{M_{mantle}} \quad (22)$$

where M_{total} is the total mass of the moon and M_{mantle} is the mass of the mantle. With ongoing time, the cooling process of the moon results in the formation of a thickening crust. Due to the incompatible character of U, Th and K these elements tend to be incorporated into the crustal material, following their specific liquid-solid distribution coefficients. This leads to their enrichment in the crust and a depletion of these elements in the mantle. The younger the crust is formed, the higher the concentration of these elements will be. Finally, during the growth process of the crust the concentration of incompatible elements exponentially decreases with depth.

2.2.7 Numerical discretization of the thermal evolution model

The finite difference formulation with the FTCS-scheme (forward in time, central in space) for the heat equation is done in spherical coordinates, assuming radial symmetry. This leads to the equation

$$\frac{T_i^{t+1}-T_i^t}{dt} = \frac{1}{\rho_i \cdot c_{P\,eff\,i}} \cdot \left(\frac{\left(\lambda_{i+\frac{1}{2}} \cdot r_{i+\frac{1}{2}} \cdot \frac{T_{i+1}^t - T_i^t}{dr} \right) - \left(\lambda_{i-\frac{1}{2}} \cdot r_{i-\frac{1}{2}} \cdot \frac{T_i^t - T_{i-1}^t}{dr} \right)}{r_i^2 \cdot dr} + \frac{H_i^t}{c_{P\,eff\,i}} \right) \quad (23)$$

For solving the temperature field at the the next time step the rearrangement results in:

$$T_i^{t+1} = T_i^t + \left(\frac{1}{\rho_i \cdot c_{P\,eff\,i}} \cdot \left(\frac{\left(\lambda_{i+\frac{1}{2}} \cdot r_{i+\frac{1}{2}} \cdot \frac{T_{i+1}^t - T_i^t}{dr} \right) - \left(\lambda_{i-\frac{1}{2}} \cdot r_{i-\frac{1}{2}} \cdot \frac{T_i^t - T_{i-1}^t}{dr} \right)}{r_i^2 \cdot dr} + \frac{H_i^t}{c_{P\,eff\,i}} \right) \right) \cdot dt \quad (24)$$

The upper boundary condition on the surface is a Dirichlet condition with the fixed temperature T_{sur}=273 K. The boundary condition in the center of the moon is a von-Neumann condition where the first derivative of the temperature is defined as 0. This corresponds to no heat flux into the centre (a spherical symmetry requirement). The density, heat capacity and thermal conductivity have been calculated every timestep. The spatial resolution of the model is 101 gridpoints, leading to a spacing dr of approximately 17 km between the gridpoints. The temporal resolution is calculated via the Courant criteria, which defines the maximal possible timestep dt as follows:

$$dt = \frac{dr^2}{2 \cdot \kappa} \quad (25)$$

Because of the permanent recalculation of ρ, c_p and λ at each time-step the

maximal Courant timestep will be reduced by a factor of 0.7 to avoid an unwanted numerical error. So the maximum time step is given by

$$dt = 0{,}7 \cdot \frac{dr^2}{2 \cdot \kappa} \quad (26)$$

In Fig. 3 a flowchart of the thermal evolution model is demonstrated.

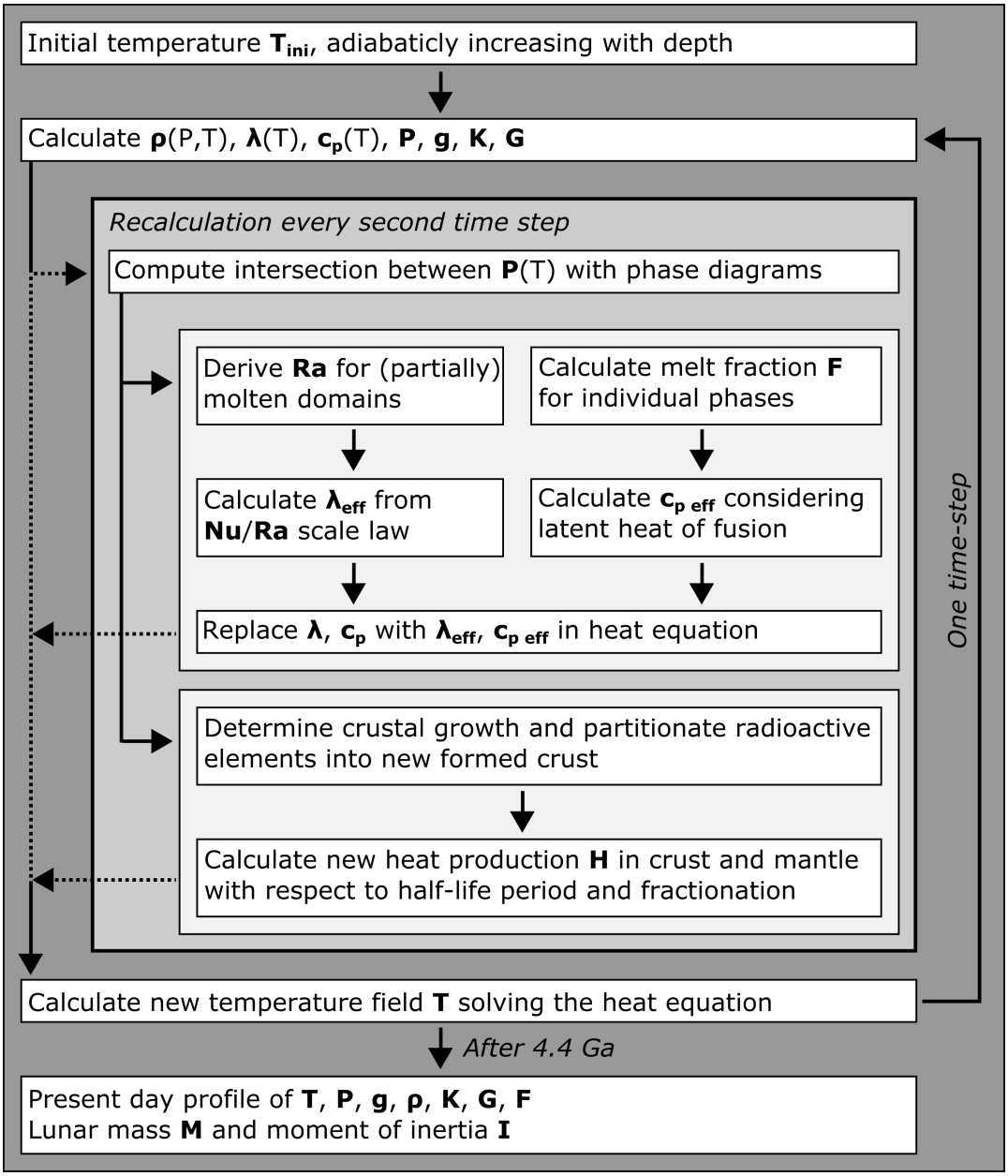

Figure 3: *Flowchart of the thermal evolution model. Note that the term crust in this chart doesn't refer to the mineralogical crust, but to the solidifying parts of the initally existing molten silicate domains.*

2.3 Tidal deformation

This chapter aims to describe the tidal deformation of the moon as a result of its orbiting around the Earth. First, in Ch. 2.3.1 tidal forces will be described in general. In Ch. 2.3.2 the deformation of an elastic body under a tidal influence will be discussed. In Ch. 2.3.3 the numerical approach how to calculate a tidal deformation and Love numbers of the Moon will be presented.

2.3.1 Tidal forces

For celestial bodies orbiting around a gravitational center like in the Earth-Moon-system or the Earth-Sun-system the gravitational acceleration is harmonically time dependent. This effect is a result of the fact that the masses are changing their positions relative to the center of mass of the system. The tidal acceleration is the gradient of the tidal potential. The tidal potential V_{tidal} on the Moon as a result of its orbiting the Earth can be obtained by:

$$V_{tid} = \frac{G_c \cdot M_E}{r'} = \frac{G_c \cdot M_E}{R} \cdot \frac{1}{\sqrt{1 + (R/r)^2 - 2 \cdot (R/r) \cdot \cos(\epsilon)}} \quad (27)$$

where G_c is the gravitation constant and M_E the mass of the earth. The distances r, r', R and the angle epsilon are explained in Fig. 4. The tidal potential can also be expressed in spherical harmonics by replacing the square root term with its expansion into the series of Legendre polynomials (Eq. 28).

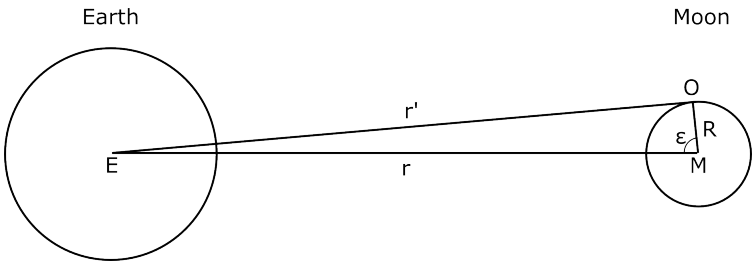

Figure 4: *Geometry for the calculation of the tides on the moon due to the Earths influence at any surface point O. E and M denote the centre of mass of each object and the angle epsilon is the angle between the line between the centres of mass and the observation point O.*

$$V_{tid} = \frac{G_c \cdot M_E}{r} \cdot \sum_{n=2}^{\infty} \left(\frac{R}{r}\right)^n P_n(\cos(\epsilon)) \quad (28)$$

The polynomial of a degree n=0 is a constant, so its gradient is zero and it can be neglected. The degree n=1 can also be discarded, because its gradient corresponds to the centrifugal acceleration of the orbiting. Thus, the tidal potential polynomials start with the degree n=2. In this work only the degree n=2 of the tidal potential will be considered. This is legitimite because the n=2 term is responsible for about 98 % of the tidal potential (Fig. 5). The tidal potential is then given as follows:

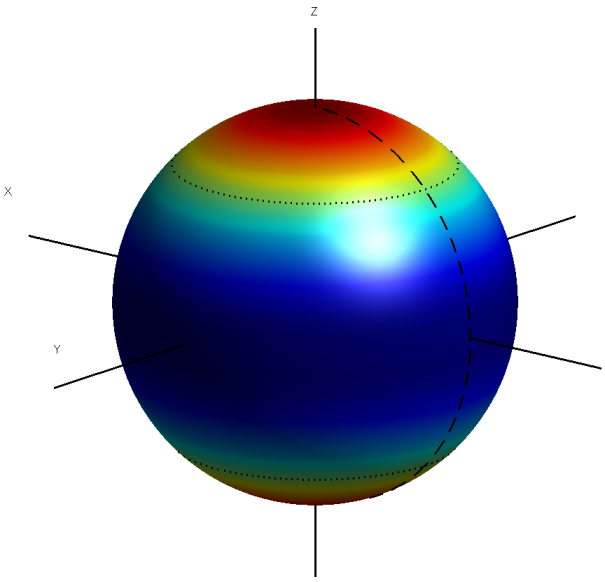

Figure 5: *Spherical harmonics - Legendre polynomial P_2, on the poles and on the equatorial line are extremes with opposite signs.*

$$V_{tid} = \frac{G_c \cdot M_E}{r} \cdot \left(\frac{R}{r}\right)^2 \cdot P_2(\cos(\epsilon)) = \frac{G_c \cdot M_E \cdot R^2}{r^3} \cdot \left(\frac{3}{2}\cos^2(\epsilon) - \frac{1}{2}\right) \quad (29)$$

The tidal acceleration is calculated from the gradient of the tidal potential V_{tid}:

$$a_R = \frac{\partial V_{tid}}{\partial R} = \frac{G_c \cdot M_E \cdot R}{r^3} \cdot \left(3\cos^2(\epsilon) - 1\right)$$

$$a_\theta = -\frac{\partial V_{tid}}{R \cdot \partial \theta} = \frac{G_c \cdot M_E \cdot R}{r^3} \cdot \left(\frac{3}{2}\sin(2 \cdot \epsilon)\right) \quad (30)$$

$$a_\lambda = -\frac{\partial V_{tid}}{R \cdot \cos(\theta) \cdot \partial \lambda} = 0$$

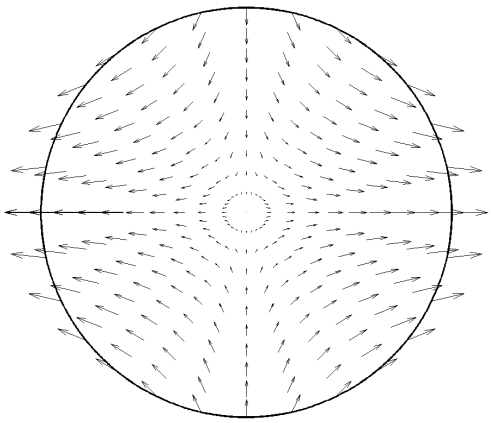

Figure 6: *Non-dimensional tidal acceleration vectors calculated from Eq. 30 (P_2-polynomial). The circle represents the surface of any celestial body. The orbiting partner is on the horizontal axis far left or right (not depicted).*

In Fig. 6 the resulting acceleration is shown.

2.3.2 Tidal deformation and Love numbers

For the description of the tidal deformation of the elastic planetary body, the dimensionless Love numbers h_n, k_n and l_n have been introduced. The index n refers to the spherical harmonic of the degree n. In the following text it is assumed that the described body is of a spherical symmetry and visco-elastic. The Love number h_n describes the the radial displacement on a bodies surface due to its tidal deformation.

$$d_{rad} = h_n \cdot \frac{V_{tid}}{g_{sur}} \quad (31)$$

The love number k_n describes the additional gravitational potential on a bodies surface due to its tidal-related relocation of mass:

$$V_{add} = k_n \cdot V_{tid} \quad (32)$$

The love number l_n, sometimes called the Shida number, is related to the horizontal displacement on a bodies surface.

$$d_{hor} = l_n \cdot \frac{\nabla_1 V_{tid}}{g_{sur}} \quad (33)$$

V_{tid} is thereby the tidal potential described in Eq. 29, g_{sur} is the surface gravitational acceleration and ∇_1 is the horizontal, spherical gradient operator. For the analytical calculation of k_2 the approach of *Remus et al (2012)* was used. In the above mentioned work the relation between the effective rigidity $\overline{\mu}$ and the k_2 Love number was derived:

$$k_2 = \frac{3}{2} \cdot \frac{1}{1+\overline{\mu}} \quad (34)$$

The effective rigidity of celestial body $\bar{\mu}$ can be obtained by integrating the shear modulus G from center to surface (*Zhang et al (2004)*):

$$\overline{\mu} = 3 \cdot \int_0^1 G(s) \cdot s^2 \, ds \quad (35)$$

where s = r/R is dimensionless radial coordinate. Since the tidal deformation is not purely elastic in nature, the shear modulus was modified to a complex shear modulus in order to account for a non-elastic component of the planetary body deformation or in other words an attenuation factor for elastic waves. Therefore, the elastic behaviour of the Moons material has been assumed to follow a Maxwellian rheology. The Maxwell relaxation time is give by

$$\tau_m = \frac{\eta}{G} \quad (36)$$

and the complex shear modulus G* is given by the expression as follows

$$G^* = \frac{i \cdot \omega \cdot G}{i \cdot \omega + \tau_m^{-1}} \quad (37)$$

where i denotes the imaginary unit and Omega the angular frequency of the tidal forcing (*Harada et al (2014)*). The complex shear modulus was inserted in Eq. 35 to obtain the effective complex rigidity $\bar{\mu}$. This results in a complex Love number k_2^* which can be used to calculate the tidal quality factor Q, describing the amount of energy lost per one tidal cycle.

$$Q = \frac{|k_2^*|}{|\Im k_2^*|} \quad (38)$$

The essential thing in this approach is the frequency dependent k_2 Love numbers which can be estimated from differing time-scale observation of a gravity anomaly on the surface of a planetary body.

2.4 Electrical conductivity

In this chapter the electical conductivity mechanisms in rocks will be shortly discussed. Afterwards, the laboratory measurements of the electical conductivity of lunar analogue materials which have been carried out for this study will be described. In the third part of this chapter the relation between the lunar magnetometer transfer function and the electrical conductivity structure of the moon is explained. At last, the numerical discretization of the inversion problem is presented.

2.4.1 Electrical conductivity of rocks and minerals

The electrical conductivity of the Earths minerals is strongly dependent on temperature and slightly dependent on pressure *(Electrical conductivity of minerals and rocks, Karato & Wang, pp. 6)* Furthermore, there is a strong effect of water content c_w on the electrical conductivity of nominally water-free minerals. Typically, the electrical conductivity increases by 1-2 magnitudes if nominally water-free olivine is compared to 50 ppm water bearing olivine *(Treatise on Geophysics Vol. 1, Romanowicz & Dziewonski, pp. 667)*. The dissolved water in nominally water-free minerals is mostly in a form of hydroxyl groups (OH^-) or protons (H^+). The temperature dependence of the electrical conductivity of minerals follows an Arrhenian law:

$$\sigma(T) = \sigma_0 \cdot e^{\frac{-E_A}{k_B \cdot T}} \quad (39)$$

where σ_0 is the preexponential factor, k_B is the Boltzmann constant and E_A the specific activation energy. The specific activation energy or enthalpy describes an energy barrier which the charge carriers have to overcome in order to transport their electrical charge to a neighboring site. These charge carriers are linked to the prevalent charge transportation process. This can be dominated either by electronic, protonic or by ionic transport mechanisms. At low

temperatures the ionic transport mechanism via protons is dominant. At higher temperatures the vacancy (lattice defect) conduction mechanism dominates the charge transport process *(Electrical conductivity of minerals and rocks, Karato & Wang, pp. 7)*.

The electrical conductivity of rocks can be calculated by using an appropriate averaging of individual mineral conductivities. Therefore, the Hashin-Shtrikman method can be applied, which gives an upper and lower bound for an isotropic multi-component material. The formulation of the Hashin-Shtrikman bounds is as follows (*Hashin & Shtrikman (1962)*):

$$\sigma_{min/max} = \left(\sum_{n=1}^{N} \frac{f_i}{\sigma_n + 2 \cdot \sigma_N} \right)^{-1} - \sigma_N \quad (40)$$

σ_n are the conductivities of the N phases and f_i their fractions, respectivelty. To obtain the lower bound σ_{min} one must sort the conductivity in decreasing order so that σ_N is the component with the lowest conductivity. For the upper bound the conductivities has to be sorted in increasing order with σ_N as the component with the highest conductivity.

For the conductivity calculation of the different mineralogical parts of the Moon the following phases and their dependencies were taken into account:

The lunar crust is composed of ortho-pyroxene and anorthite as described in Ch. 2.1. For these two phases measurements with lunar analogue materials were carried out to derive the electrical conductivity as a function of temperature. The measurements will be discussed more specific in the next chapter.

For the upper and lower lunar mantle only the main phases olivine, ortho-pyroxene, clino-pyroxene and spinell/garnet from other publications were taken into account. Except of clino-pyroxene, all of them are not only temperature dependent but also dependent on the water content c_w.

For the lunar core the conductivity was assumed to be constant at 10^6 S/m (*de Koke et al (2012)*).

2.4.2 Electrical conductivity measurements of lunar analogue materials

Two types of rocks are typical for the lunar crust: anorthite and basalt. Anorthite is a rock dominated by Ca-rich feldspars. On the lunar surface anorthitic zones appear bright. The lunar basalts, the material of the dark maria, differ from the basalts known on the Earth. The lunar basalts are strongly enriched in titanium which increases the electrical conductivity. Due to an absence of data in literature about the electrical conductivity of anorthite and Ti-rich basalts, laboratory conductivity measurements for these two rocks were carried out. The measurements have been done in a piston cylinder press (Fig. 7) with the use of the electrical impedance spectroscopy method at different temperatures and constant pressures in order to derive the temperature-dependent electical conductivity in the form of Eq. 40.

For the measurements process the samples were milled to fine powder (~50 µm) and heated inside the press for ~100 h at temperatures below their solidus for sintering. The electical conductivtity was determined in intervals of 40°C over a temperature range given in Table 1:

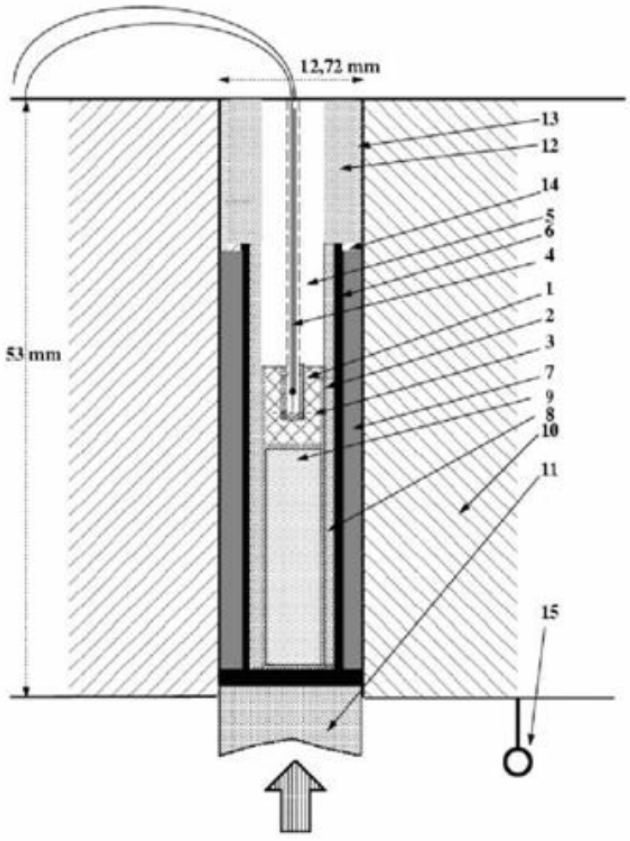

Figure 7: *Measurement of the electical conductivity in a pistion cylinder press: 1 and 2 Mo-film, 3 sample, 4 thermocouple, 5 Al_2O_3-ceramic, 6 graphit heating, 7 CaF_2-mantle, 8 BN-mantle, 9 BN-cap, 10 metal core, 11 metal piston, 12 metal cap, 13 BN- or pyrophyllite, 14 copper ring, 15 ground electrode*

		Anorthite	Troktolit
Temp. range [°C]	from	270	220
	to	1300	1100
Pressure [GPa]		1.0	0.6

Table 1: *Temperature range and pressure for the conductivity measurements.*

The measurement of the electical conductivity has been done with alternating current in the frequency range from 0.05 Hz to 250 kHz at 64 frequencies. The
755 results of the measurements are depicted in Table 2, Fig. 8 and Fig. 9.

	T.-range [°C]	S_0 [S/m]	E_A [eV]
Anorthit	200...910	82,3	1,25
	910...1300	507,8	1,39
Troktolit	200...820	0,35	0,79
	820...1100	26,8	1,09

Table 2: *Measurement results: The pre-exponential factor S_0 and the activation energy E_A are only valid in the given temperature ranges.*

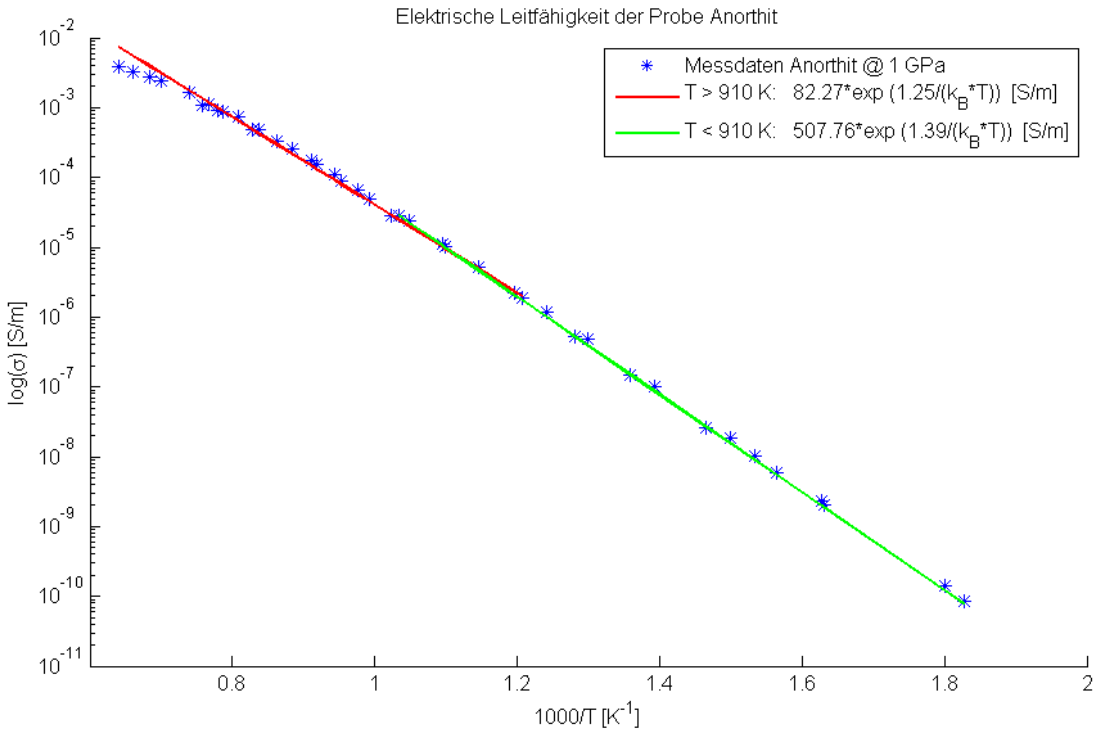

Figure 9: *Results of the anorthite sample measurements.*

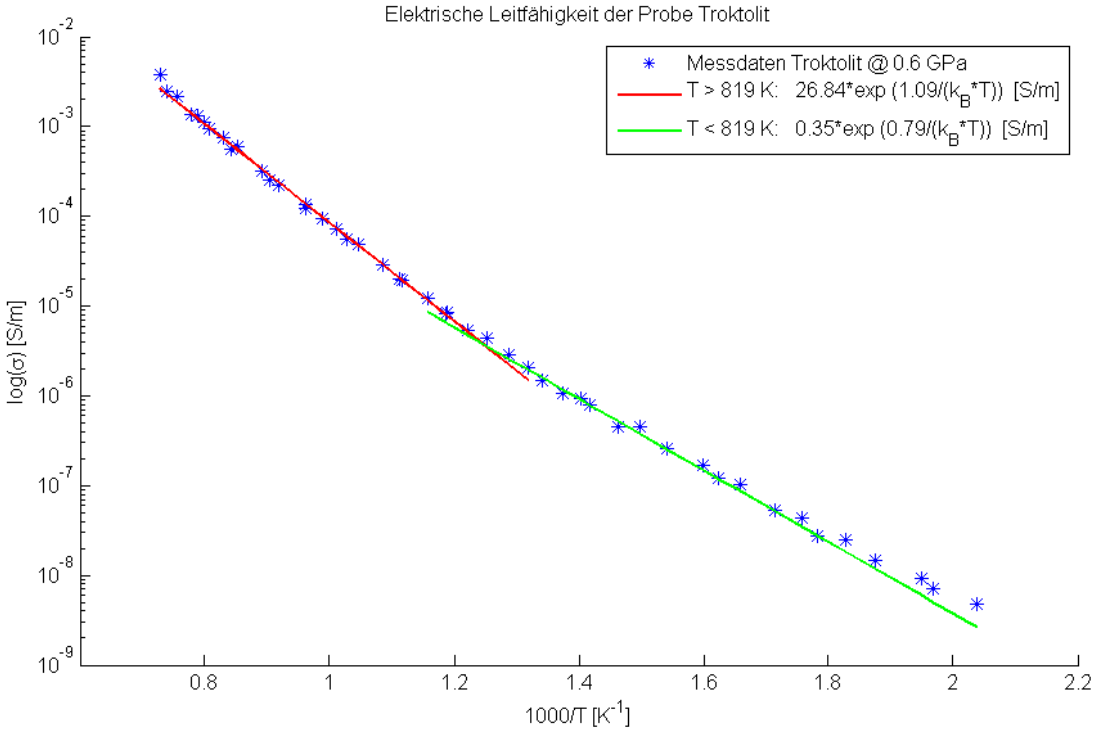

Figure 8: *Results of the troktolite measurements.*

2.4.3 Magnetometer measurements

During NASAs Apollo programm magnetometers were dispatched on the lunar surface. Theses magnetometers recorded the magnetic field as a function of time. The external magnetic field variations penetrating the Moons surface comply to a diffusion process due to induction processes. The induction results in electrical currents, the amplitude of which depends on the conductivity of a material. These currents again create a secondary magnetic field, which can be observed on the surface. This process can be described by using the first three quasi-static Maxwell equations (Eq. 41) and Ohm's law (Eq. 42).

$$\nabla \times \vec{H} = \vec{j}$$

$$\nabla \times \vec{E} = -\frac{\partial B}{\partial t} \quad (41)$$

$$\nabla \cdot \vec{B} = 0$$

with $\overline{H}$ as the magnetic field vector, $\bar{j}$ is the current density vector, $\overline{E}$ is the electric field vector and $\overline{B}$ is the magnetic flux density vector.

$$\vec{j} = \sigma \cdot \vec{E} \quad (42)$$

Inserting the Eq. 42 into the first Maxell equation results in

$$\nabla \times \vec{H} = \sigma \cdot \vec{E} \quad (43)$$

After applying the rotation operator on both sides of Eq. 43 one can equate the result with the second Maxwell equation:

$$\nabla \times (\nabla \times \vec{H}) = \sigma \cdot \nabla \times \vec{E} = -\sigma \cdot \frac{\partial \vec{B}}{\partial t} \quad (44)$$

Assuming that the relative magnetic permeability $\mu_r=1$, the relation between $\overline{B}$ and $\overline{H}$ is $\overline{B} = \mu_0 \cdot \overline{H}$. Than Eq. 44 can be written as follows:

$$\nabla(\nabla \cdot \vec{B}) - \nabla^2 \vec{B} = -\frac{\sigma}{\mu_0} \cdot \frac{\partial \vec{B}}{\partial t} \quad (45)$$

As the third Maxwell equation states that the divergence of $\overline{B}$ is zero, the equation reduces to

$$\nabla^2 \vec{B} = \frac{\sigma}{\mu_0} \cdot \frac{\partial \vec{B}}{\partial t} \quad (46)$$

Further one can transform the Eq. 46 from the time domain to the frequency domain by inserting an harmonic time-dependence of vector $\overline{B}$. The time derivative then disappears.

$$\nabla^2 \vec{\Lambda} = i \cdot \omega \cdot \sigma \cdot \mu_0 \cdot \vec{\Lambda} \quad (47)$$

ω is the angular frequency of the magnetic field variation $\overline{B}$ and Λ are the Fourier series coefficients of the magnetic field. Eq. 47 now represents a Poisson equation. For a 1D-radial conductivity structure the spherical transformation of this equation gives

$$\frac{\partial^2 \Lambda}{\partial r^2} - i \cdot \omega \cdot \sigma(r) \cdot \mu_0 \cdot \Lambda = 0 \quad (48)$$

Typically, magnetometer transfer functions are expressed in terms of the so called C-response:

$$|C(\omega)| = \frac{R}{2} \cdot \Gamma(\omega) \quad (49)$$

with $\Gamma(\omega)$ as the ratio of the sum of external and induced field to external field:

$$\Gamma(\omega) = \left| \frac{B_{ext}(\omega) + B_{ind}(\omega)}{B_{ext}(\omega)} \right| = \left| \frac{R}{2} \cdot \frac{\partial \Lambda(\omega)}{\partial r} \right|_{r=R} \quad (50)$$

An apparent resistivity can then be calculated which can be compared to the observed apparent resistivity.

$$\rho_A(\omega) = \omega \cdot \mu_0 \cdot |C(\omega)|^2 = \frac{\omega \cdot \mu_0 \cdot R^2}{4 \cdot \Gamma^2(\omega)} \quad (51)$$

The observed frequency-dependent apparent resistivities can be found in Ch. 2.5.2.

2.4.4 Numerical discretization of electrical conductivity model

For the calculation of the lunar transfer function at first the conductivity profile of the Moon is derived from the temperature profile (calculated selenotherm) resulted from the thermal evolution modeling. The estimation of the electrical conductivity from the known temperature and mineralogical composition by using the Hashin-Shtrickman bounds results in an upper and a lower radial conductivity profiles. These profiles have then been used to calculate the diffusion process of electromagnetic waves according to Eq. 48 for different frequencies. For solving such a partial differential equation sophisticated boundary conditions have to be applied. These conditions are Dirichlet conditions on the upper and lower boundaries with defined values of the desired function Λ. For the upper boundary, the lunar surface, the value was chosen to be $\Lambda=1$. For the lower boundary, the magnetic field is assumed to vanish there, and a value of $\Lambda=0$ is set, where Λ is the magnetic field strength in the frequency domain.

2.5 Inversion strategy

In this chapter the used inversion technique is presented. First of all, the functional principle of the Downhill Simplex algorithm is presented in Ch. 2.5.1, then in Ch. 2.5.2 the observed and calculated parameters which need to be fitted are described and finally the calculation and weighting of the model-data-to-observed-data misift will be outlined.

2.5.1 Downhill Simplex algorithm

The Downhill Simplex algorithm is an inversion technique which gets along without the use of partial derivatives of the misfit function with respect to the fitting parameters in order to find a global minimum of the misfit function. This makes it a very robust and stable inversion algorithm. The disadvantage of the Downhill Simplex algorithm is that it converges also to local minima and that it is quite slow compared to other inversion techniques. The minima that are encountered by the inversion are typically linked to the misfit value describing the deviation of a model to the observed dataset, the above mentioned misfit function. By repeating a series of Downhill Simplex runs with different starting conditions a global minimum i.e. a minimal misfit between a model and the observations can be identified.

The working principle of the Downhill Simplex algorithm: At the beginning of a Downhill Simplex run a so-called simplex has to be formed. For function with P parameters, P+1 parameter combinations are chosen arbitrarily. Each parameter combination is termed a point Π, referring to a position in the P-dimensional parameter space. For each point a model computation is carried out with the corresponding parameters and a misfit-value is calculated. After that, the algorithm enters a loop:

1. Dermination of the best Π_0, the second-worst Π_{P-1} and the worst point Π_P
2. Reflect (Eq. 53) the worst point at geometrical centre Π_M (Eq. 52) of the remaining points giving the reflected point Π_R

3. Repeat the reflection of the worst point at Π_M but with an expansion factor β (Eq. 54) resulting in the point Π_E
4. If Π_R or Π_E is better than Π_0 replace Π_0 by Π_R or Π_E, respectively and go back to step 1
5. If Π_R is better than Π_{P-1}, replace Π_{P-1} by Π_R and go back to step 1
6. Define the point Π_W as the better point between Π_R and Π_P, then move the point Π_W towards the remaining points (contraction) giving Π_C (Eq. 55)
7. If Π_C is better than Π_P, replace Π_P by Π_C and go back to step 1
8. Compress the simplex along all dimension towards Π_0 (Eq. 56) and go back to step 1

A repetition of this loop continues until either a convergence criteria is satisfied or a certain number of iterations is exceeded.

The geometrical centre Π_M in step 2 and step 3 is given by

$$\Pi_M = \frac{1}{P} \cdot \sum_{i=0}^{P-1} \Pi_i \quad (52)$$

The reflected point Π_R in step 2 is calculated according

$$\Pi_R = n_1 \cdot (\Pi_M - \Pi_P) + \Pi_M \quad (53)$$

The expanded point Π_E in step 3 is given with

$$\Pi_E = n_2 \cdot (\Pi_M - \Pi_P) + \Pi_M \quad (54)$$

For the contracted point Π_C the equation reads

$$\Pi_C = n_3 \cdot (\Pi_M - \Pi_W) + \Pi_W \quad (55)$$

For the compression all points Π_i from i=1 to P are replaced by new points Π_i^{new} as followed

$$\Pi_i^{new} = n_4 \cdot (\Pi_0 - \Pi_i) + \Pi_i \quad (56)$$

The parameters n_1, n_2, n_3 and n_4 are scaling parameters for the reflection, expansion, contraction and compression, respectively. There values are given in Table 3.

Parameter	n_1	n_2	n_3	n_4
Value	1	2	0.9	0.5

Table 3: *Coefficients for reflection, expansion, contraction and compression.*

2.5.2 Observed data and parameters

Four observed properties were chosen to be fitted: the lunar mass, its moment of inertia, the magnetometer transfer function and the monthly Love number k_2 related to the 27-day orbital cycle of the Earth-Moon-system. For these four observables five parameters can be adjusted: the initial temperature of the Moon after its accretion, the depth of the crust-mantle boundary, the depth of the upper- to lower-mantle boundary, the radius of the lunar core and the water content of the lunar mantle minerals.

The lunar mass and inertia:

The lunar mass and its inertia are well determined due to the numerous astronomical observations of the orbitation of the Earth-Moon-system and the orbitation of satellites around the Moon. The reference for the lunar mass and the moment of inertia the values from *Williams et al (2014)* have been adopted (Table 4).

	Value	Source
M_{obs}	$7.3463 \cdot 10^{22}$ kg	*Williams et al (2014)*
J_{obs}	0.393112	*Williams et al (2014)*

Table 4: *Reference values.*

The calculated mass and moment of inertia of the model is affected by three parameters, namely of the above mentioned locations of the mineralogical boundaries of crust, mantle and core.

Magnetometer transfer-function:

For the reference magnetometer transfer function the calculated frequency dependent apparent resistivities from *Hobbs et al (1983)* have been used. The authors used the Apollo 15 surface magnetometer measurements to derive the transfer function.

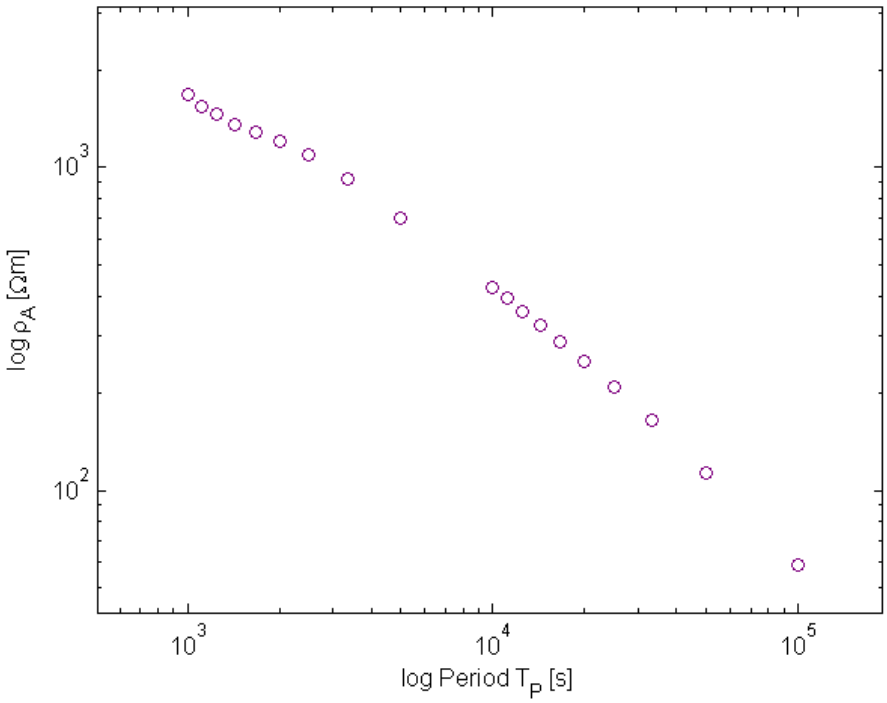

Figure 10: *Apparent resistivities from Hobbs et al (1983) based on the Apollo 15 surface magnetometer measurements.*

The calculated magnetometer transfer function is sensitive to all of the five parameters. The depth location of the different mineralogies affects the conductivity as well as the temperature and the water content of the mantle materials.

Monthly k_2:

The reference value of k_2 was taken from *Williams et al (2014)* (Table 5).

	Value	Source
$k_{2\ obs}$	0.02422	*Williams et al (2014)*

Table 5: *Reference values.*

The model Love number k_2 is controlled by all five parameters, too. For the calculation of the complex shear modulus a temperature and water dependent viscosity of minerals is used. Further the unrelaxed elastic moduli are dependent on temperature. The depth location of the crust, mantle and core boundaries with their different mineralogical compositions also influences the rigidity of the Moon and therefore the Love number k_2.

2.5.3 Misfit calculation and weighting

For the misfit function between the observed and the modeled parameter values a simple deviation calculation has been applied:
For the lunar mass M, the moment of inertia J and the k_2 Love number the misfit function is given as followed:

$$m_M = \sqrt{\frac{\left(M_{obs} - M_M\right)^2}{M_{obs}^2}}$$

$$m_J = \sqrt{\frac{\left(J_{obs} - J_M\right)^2}{J_{obs}^2}} \quad (57)$$

$$m_{k_2} = \sqrt{\frac{\left(k_{2\,obs} - k_2\right)^2}{k_{2\,obs}^2}}$$

For the magnetometer transfer function the logarithmic deviation has been calculated. This is because the transfer function varies over few orders of magnitudes.

$$m_{TF} = \sum_{n=1}^{N} \sqrt{\frac{\left[\log_{10}(TF_{obs}(n)) - \log_{10}(TF(n))\right]^2}{\left[\log_{10}(TF_{obs}(n))\right]^2}} \quad (58)$$

Thereby N denotes the number of frequencies of the observed transfer function. The overall misfit is given by the sum of all misfits:

$$m_{tot} = m_M + m_J + m_{k_2} + m_{TF} \quad (59)$$

In Fig. 11 the whole inversion procedure is shown as flowchart.

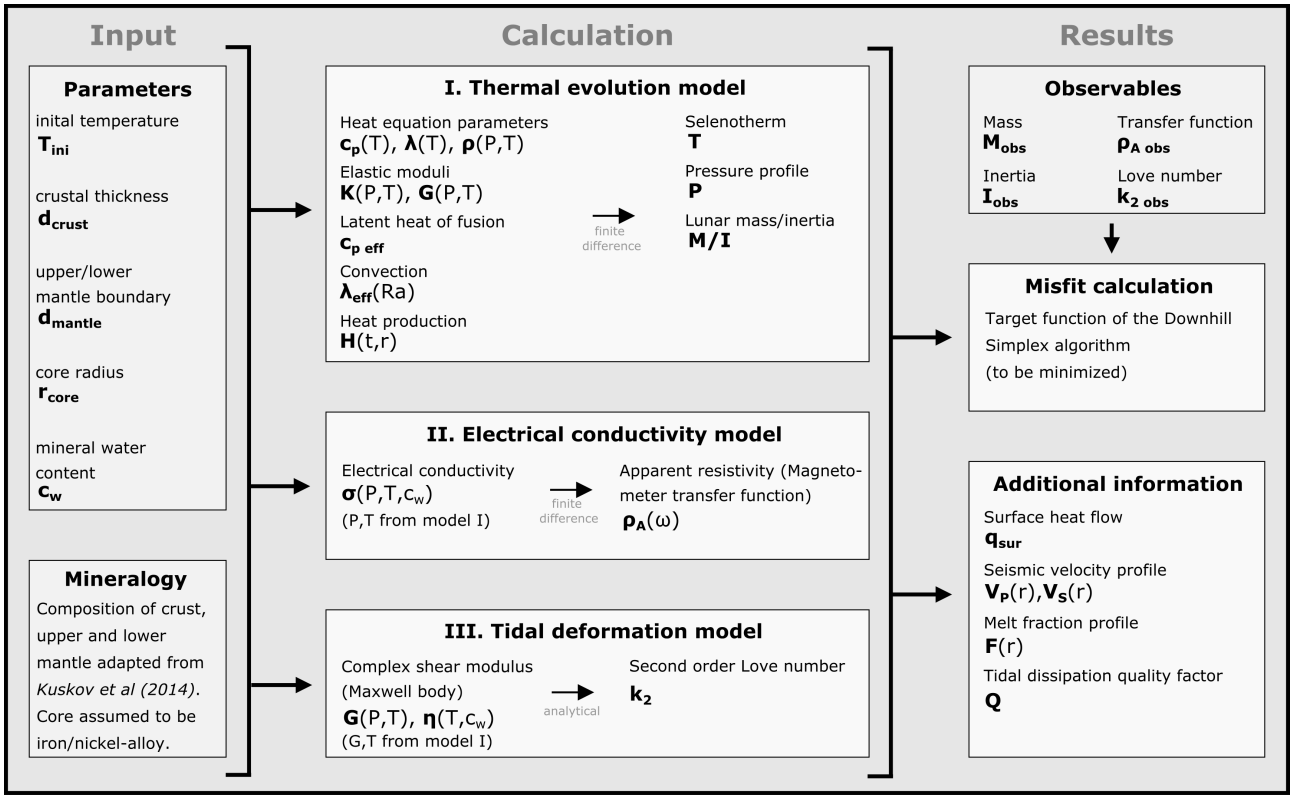

Figure 11: *Flowchart of the inversion process.*

2.6 Definition of Variables and Parameters

1055

Symbol	Value	Unit	Description
α		1/K	thermal expansivity
β	0.2		Nu/Ra coefficient (spherical)
γ	2.1		Nu/Ra coefficient (spherical)
η		Pa·s	viscosity
κ		$m \cdot s^{-2}$	thermal diffusivity
λ		$W \cdot m^{-1} \cdot K^{-1}$	thermal conductivity
λ_{eff}		$W \cdot m^{-1} \cdot K^{-1}$	effective thermal conductivity
ρ		$kg \cdot m^{-3}$	density
ρ_A		$\Omega \cdot m$	apparent resistivity
$\rho_{A\ obs}$		$\Omega \cdot m$	observed apparent resistivity
σ		$S \cdot m^{-1}$	electrical conductivity
σ_0		$S \cdot m^{-1}$	pre-exponential factor for conductivity
σ_{cw}		$S \cdot m^{-1}$	pre-exponential factor for conductivity
τ		Ga	half life period of radioactive isotopes
ω		s^{-1}	tidal frequency
E_A		eV	activation energy for conductivity
E_{cw}		eV	activation energy for conductivity
E_{decay}		MeV	decay energy of radioactive isotopes
F			melt fraction
G		Pa	shear modulus
G_0		GPa	reference shear modulus
dG/dP			pressure derivative of shear modulus
dG/dT		GPa/K	temperature derivative of shear modulu
H		$W \cdot kg^{-1}$	heat production
H_0		$W \cdot kg^{-1}$	specific heat production
I		$kg \cdot m^2$	moment of inertia
J			non-dimensional moment of inertia
J_{obs}			observed moment of inertia (non-dim.)
K		Pa	bulk modulus
K_0		GPa	reference bulk modulus
dK/dP			pressure derivative of bulk modulus
dK/dT		GPa/K	temperature derivative of bulk modulus
L		$J \cdot kg^{-1}$	latent heat of fusion
M_{total}		kg	lunar mass
M_{obs}		kg	observed lunar mass
N_A	$6.023 \cdot 10^{23}$	mol^{-1}	Avogadro constant
Nu			Nusselt number

Table 6: *Table of the used variables and parameters. The red marked entries are observed values.*

Symbol	Value	Unit	Description
P		Pa	pressure
Q			tidal quality factor
R	$1.737 \cdot 10^{6}$	m	lunar radius
R*	8.3145	$J \cdot K^{-1} \cdot mol^{-1}$	gas constant
Ra			Rayleigh number
Ra_c	1296		critical Ra
T		K	temperature
T_{ini}		K	initial temperature
T_{sur}	273	K	surface temperature
[X]		ppm	isotope concentration
$[X]_{chondrit}$		ppm	chondritic isotope concentration
c_P		$J \cdot kg^{-1} \cdot K^{-1}$	heat capacity
$c_{P\ eff}$		$J \cdot kg^{-1} \cdot K^{-1}$	effective heat capacity
c_X			coefficients for heat capacity
c_w		ppm	water content of minerals
d_{crust}		km	thickness of crust
d_{mantle}		km	depth of boundary upper/lower mantle
dr	1737	m	radial step
dt		s	time step
e	$1.602 \cdot 10^{-19}$	C	electron charge
f			fraction of phase
i			spatial index
k_2			Love number
$k_{2\ obs}$			
k_B			Boltzmann constant
r		m	radius
r_{core}		km	radius of core
t		Ga	time

Table 7: *Table of the used variables and parameters. The red marked entries are observed values. The blue marked entries are fitting parameters.*

3 Inversion Results

Altogether, 889 Downhill Simplex runs were carried out, resulting in 825 different local minima that have been found. Each Downhill Simplex started with differing, randomly chosen starting parameters. In the following figures the inversion results are shown in 2D projections of the five-dimensional parameter space. The misfit according to Eq. 59 is color coded from red (bad) to green (good), with the three best models in blue. Finally, the inversion resulted in a narrow parameter range corresponding to an optimal fit of modeled to observed data.

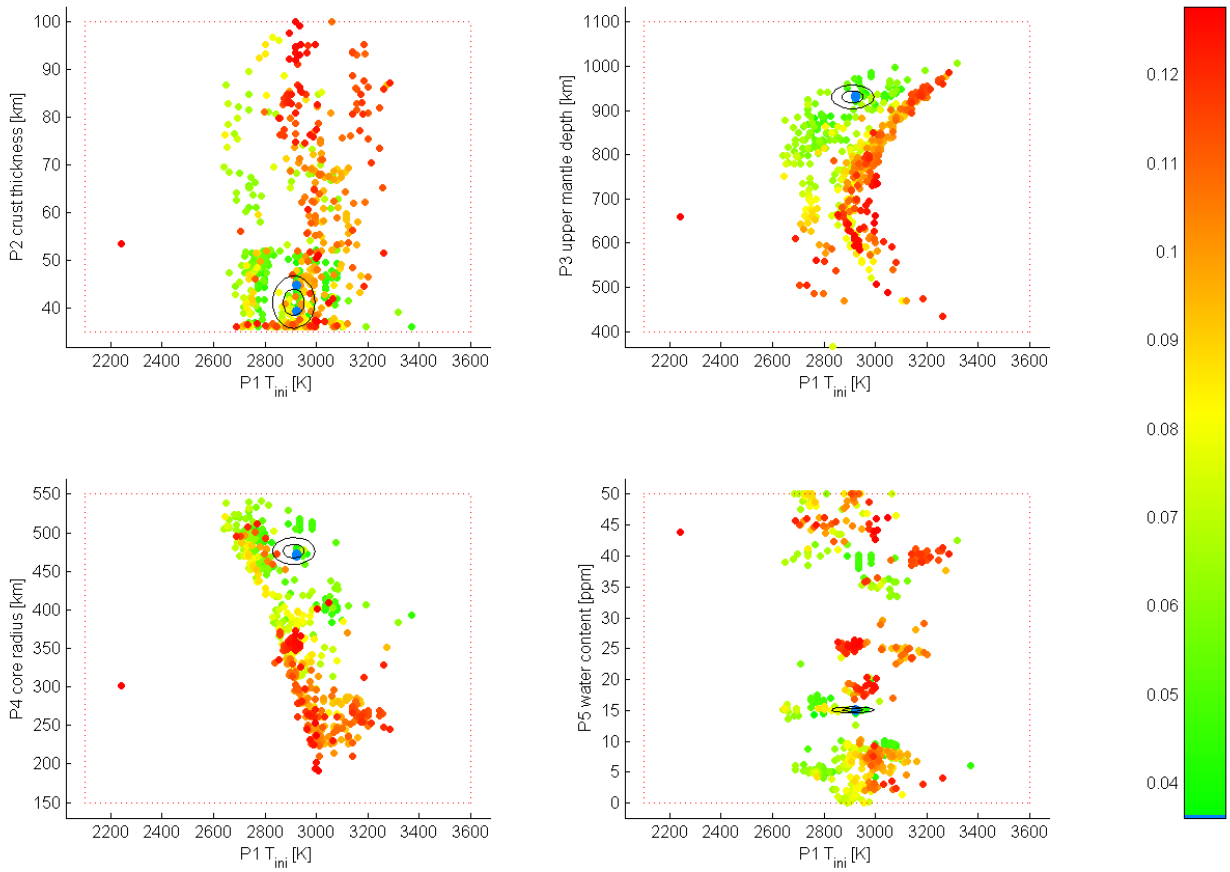

Figure 12: *2D slices of the five-dimensional parameter space. Parameter P1 "inital temperature" versus all other parameters. Each point corresponds to a local minima found by the downhill simplex algorithm. The misfit of the models is color coded. The three best models are the blue dots. The red dotted rectangle represent the parameter boundaries for the Downhill Simplex. The ellipses depict the 1σ- and 2σ-environment calculated from the 15 best models.*

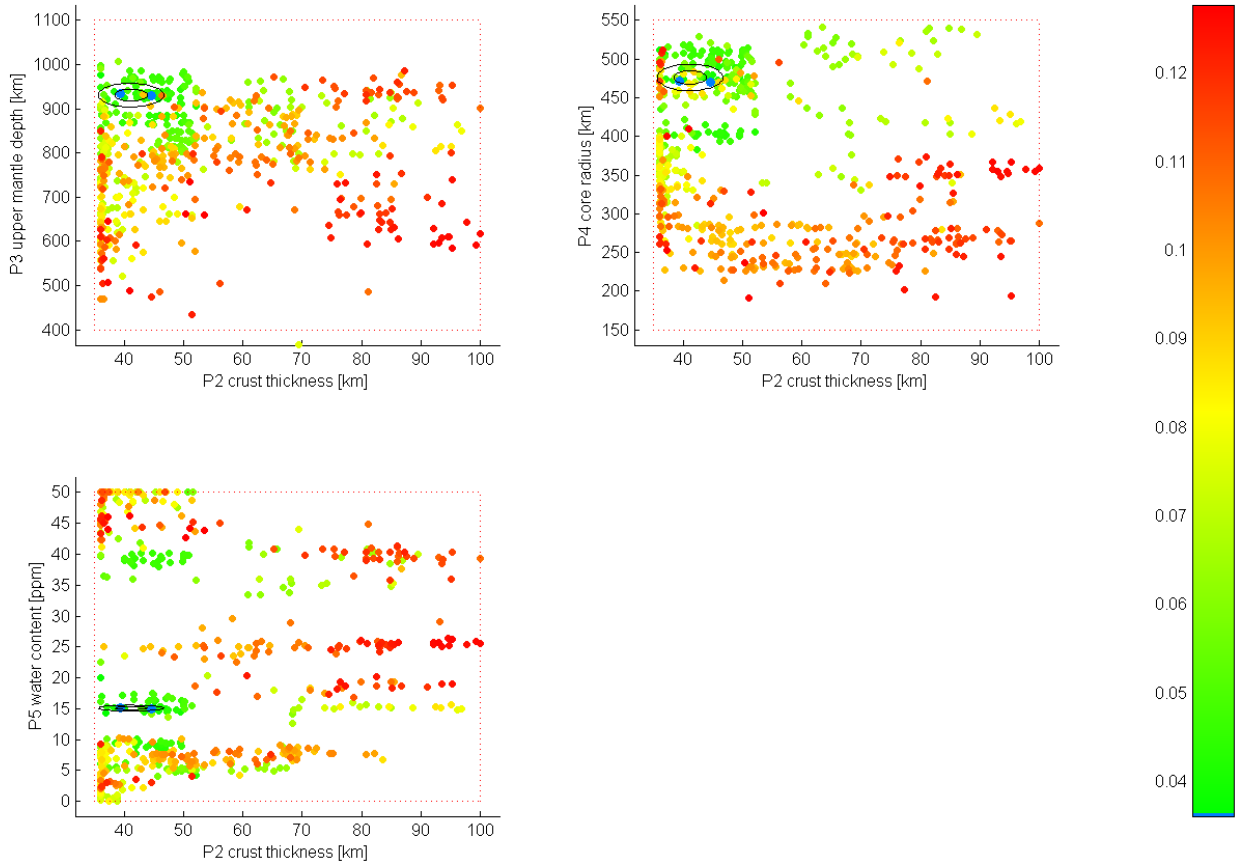

Figure 13: *2D slices of the parameter space. Second parameter "P2 crust thickness" versus P3, P4 and P5.*

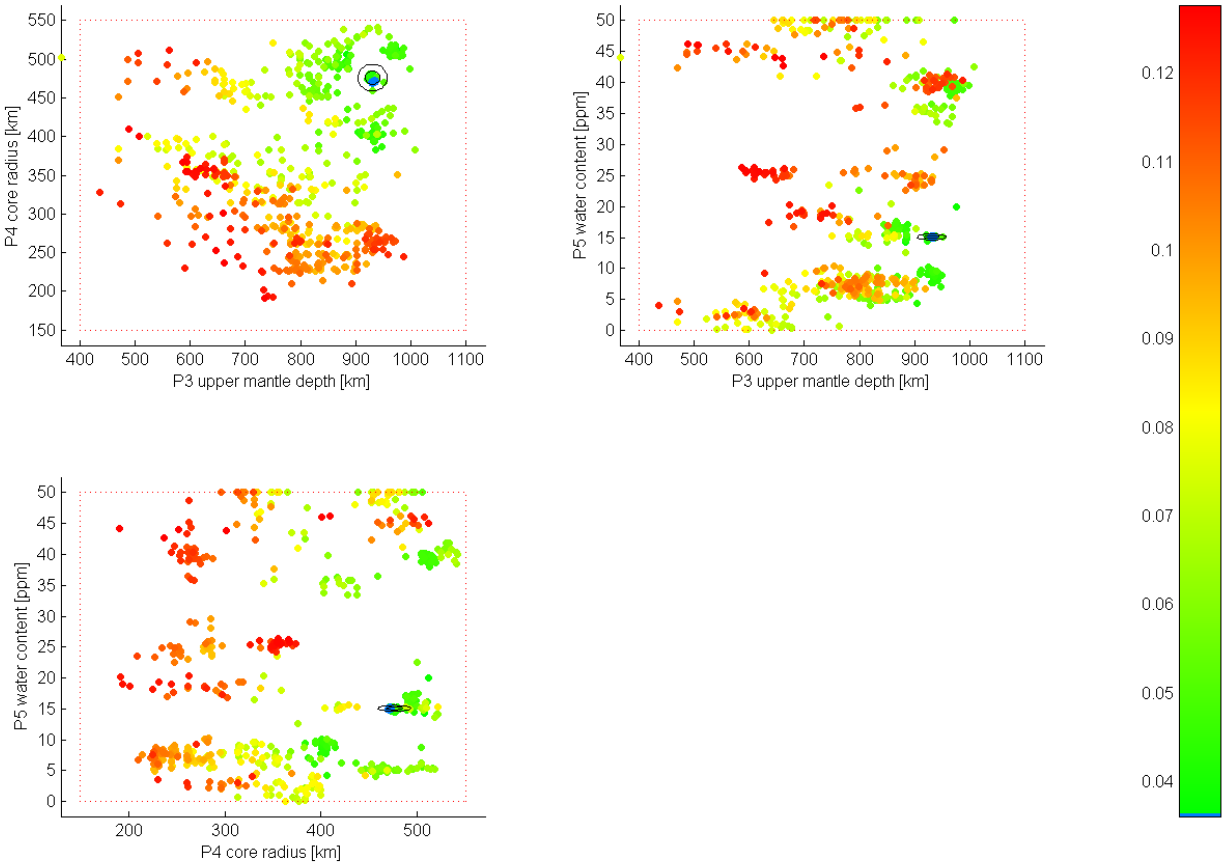

Figure 14: *2D slice of the parameter space. Parameter P3 "upper mantle boundary" versus P4 and P5. Parameter P4 "core radius" versus P5.*

The optimal parameters to fit the model to the observed data are as follows:

	T_{ini} [K]	d_{crust} [km]	d_{mantle} [km]	r_{core} [km]	c_w [ppm]
Value	2910 ±40	45 ±3	925 ±14	475 ±9	15 ±3

Table 8: *Parameters of the best model.*

On the following pages profiles of different properties are shown for the best model.

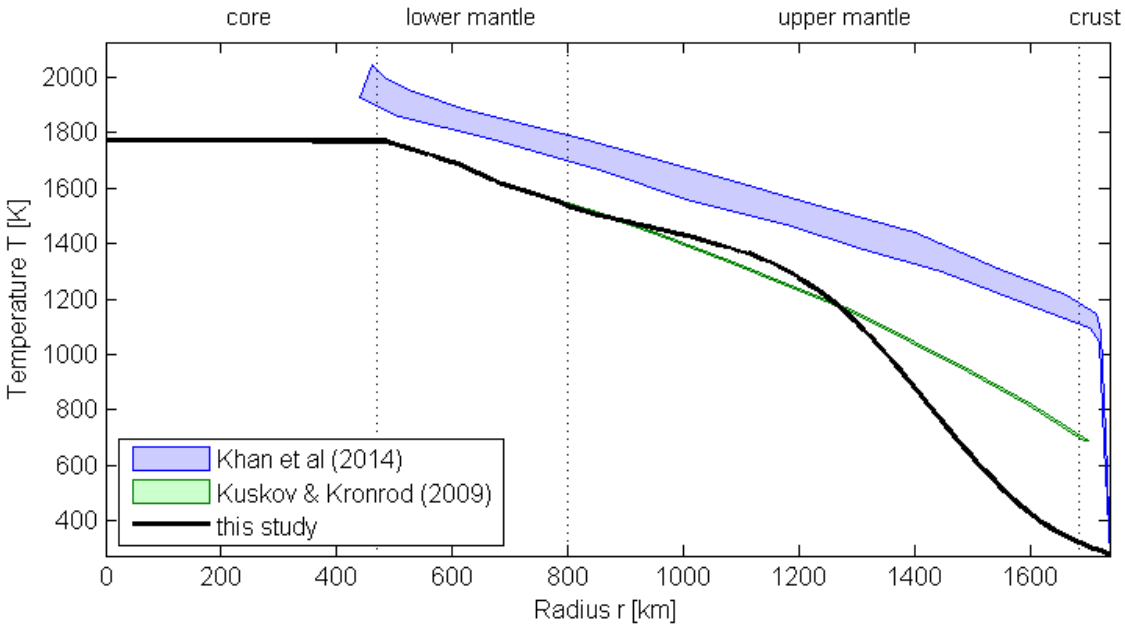

Figure 15: *The selenotherm derived from the best model. The blue area marks the upper and lower bounds for the selenotherm derived from Khan et al (2014), the green line is the mantle selenotherm from Kuskov & Krondrod (2009).*

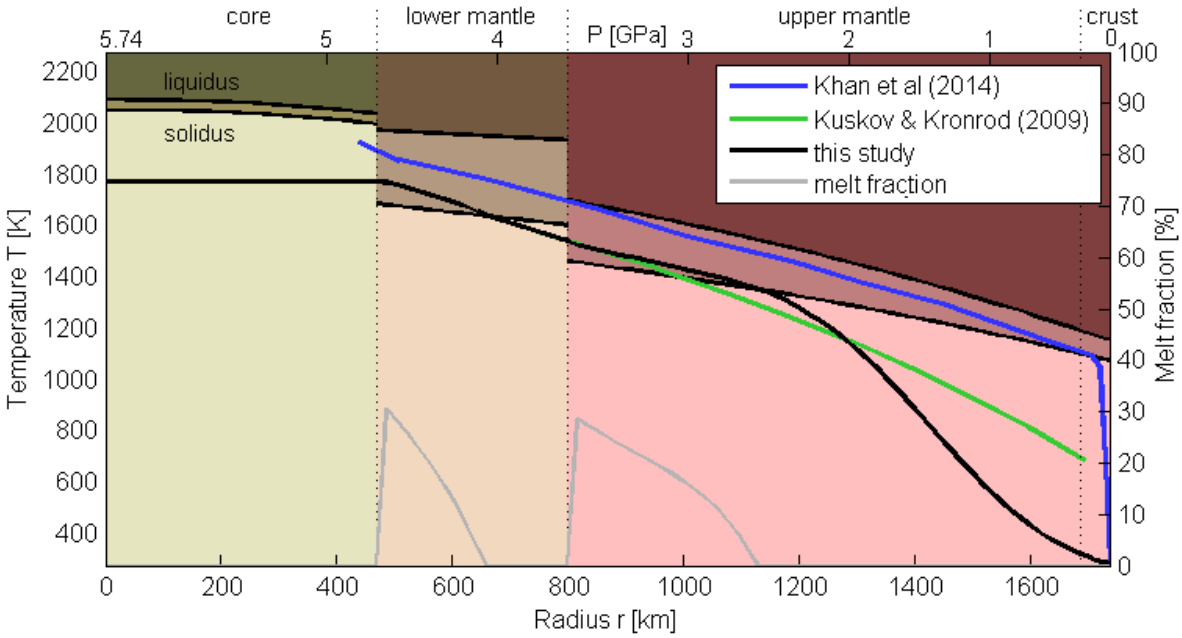

Figure 16: *Intersection of the temperature gradient with the solidus and liquidus of the different phases. ● Iron/Nickel, ● Peridotite, ● Pyroxenite. The dark colored area corresponds to conditions above liquidus, the light colored area is below the solidus. The area inbetween was used to calculate the melt fraction.*

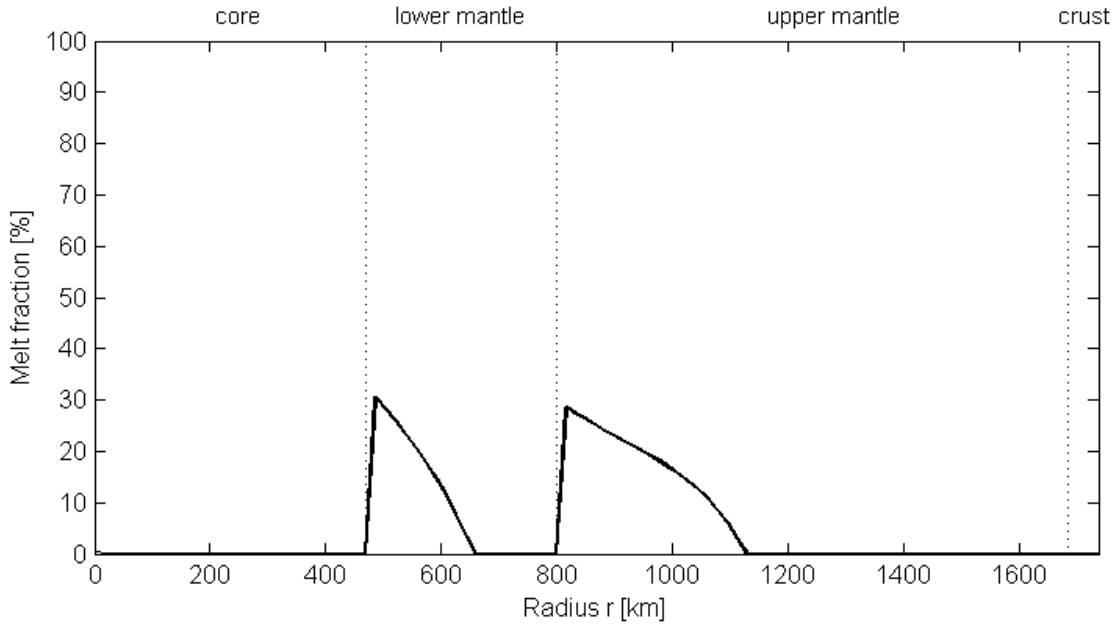

Figure 17: *Melt fraction versus depth. In the lower regions of the upper and the lower mantle partial melt of up to 30%.*

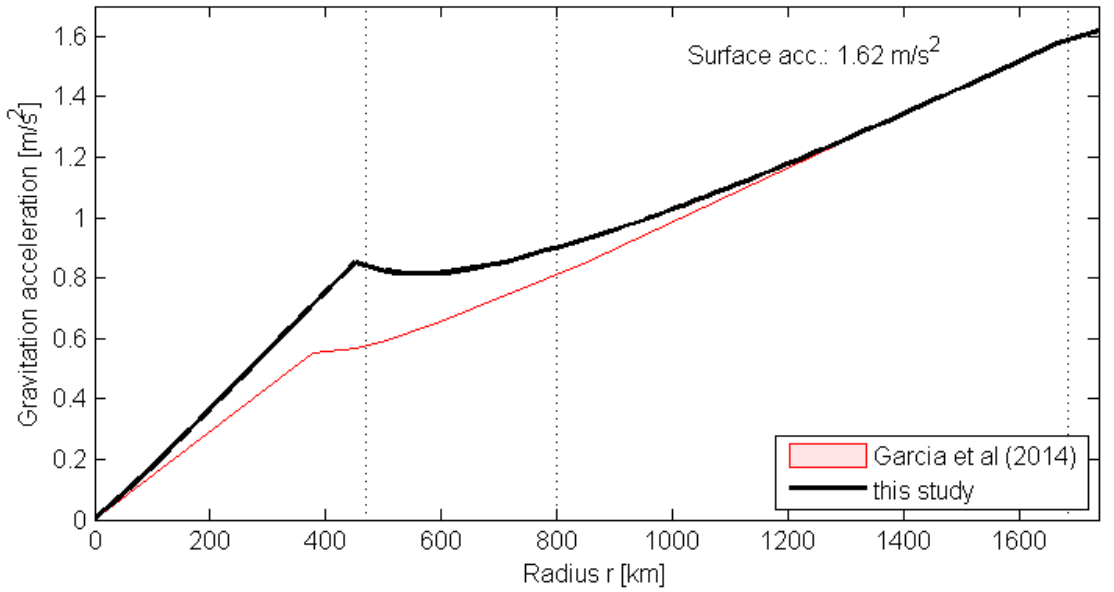

Figure 18: *Gravitation acceleration versus radius. The reference model suggested by Garcia et al (2014) is depicted as red line.*

1110

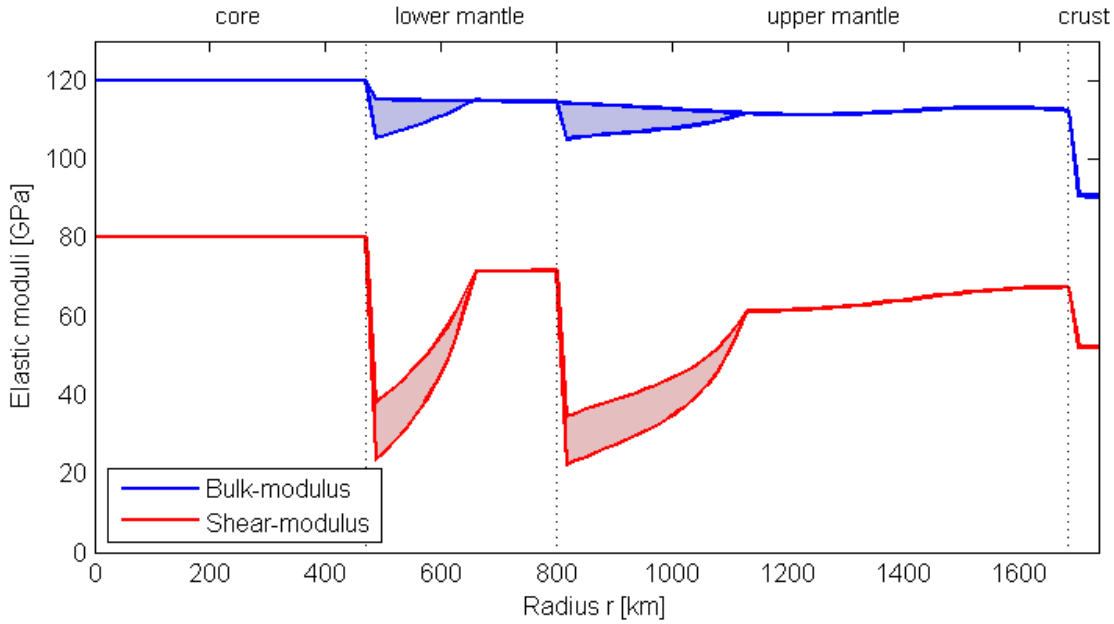

Figure 19: *Profiles of elastic moduli with upper and lower bounds. The blue line is the bulk-modulus, the red line is the shear-modulus. The great difference between the upper and lower bound for the shear-modulus corresponds to the partially molten domains.*

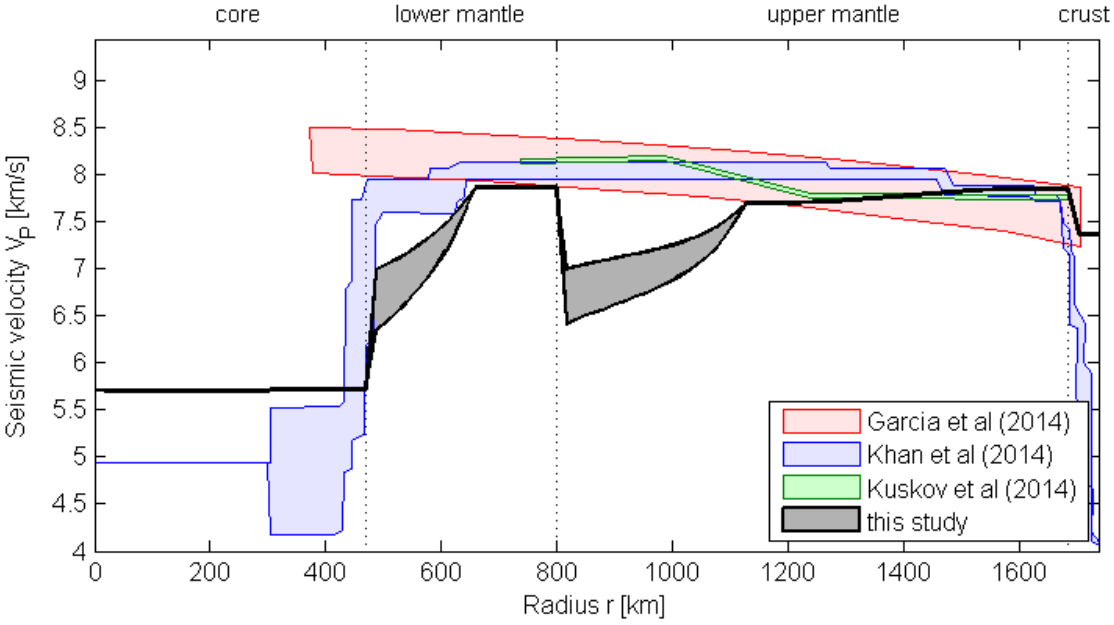

Figure 20: *Profiles for P-wave velocities with upper and lower bounds. In black/gray the results of this study, in red the proposed upper and lower bounds from the reference model by Garcia et al (2014), in blue the results from Khan et al (2014) and in green the results from Kuskov et al (2014).*

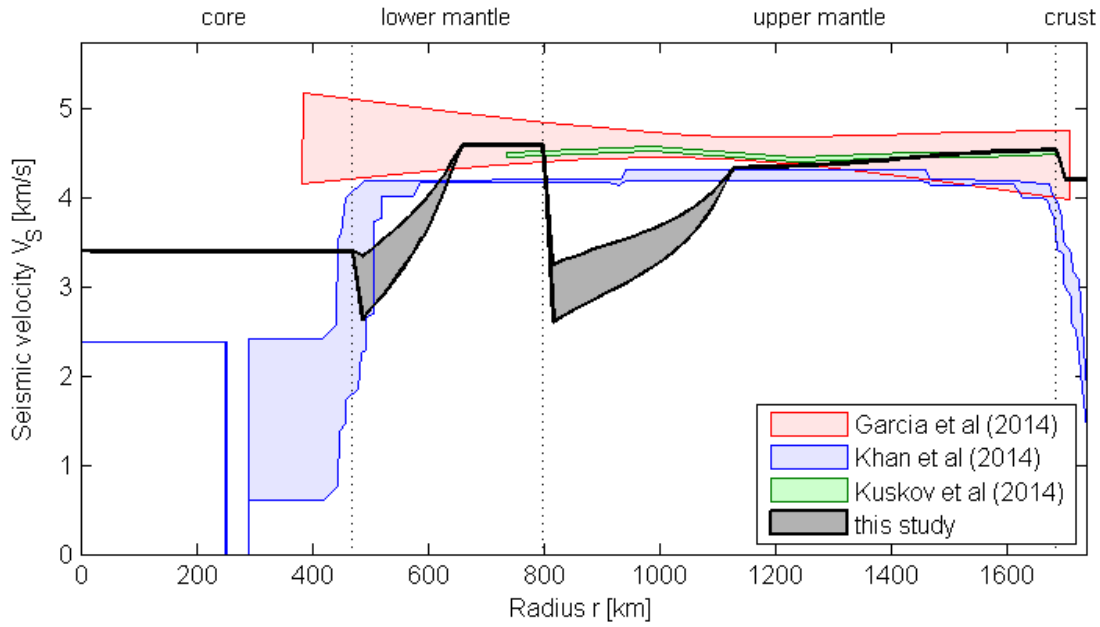

Figure 21: *Profiles for S-wave velocities with upper and lower bounds. In black/grey the results of this study, in red the proposed upper and lower bounds from the reference model by Garcia et al (2014), in blue the results from Khan et al (2014) and in green the results from Kuskov et al (2014).*

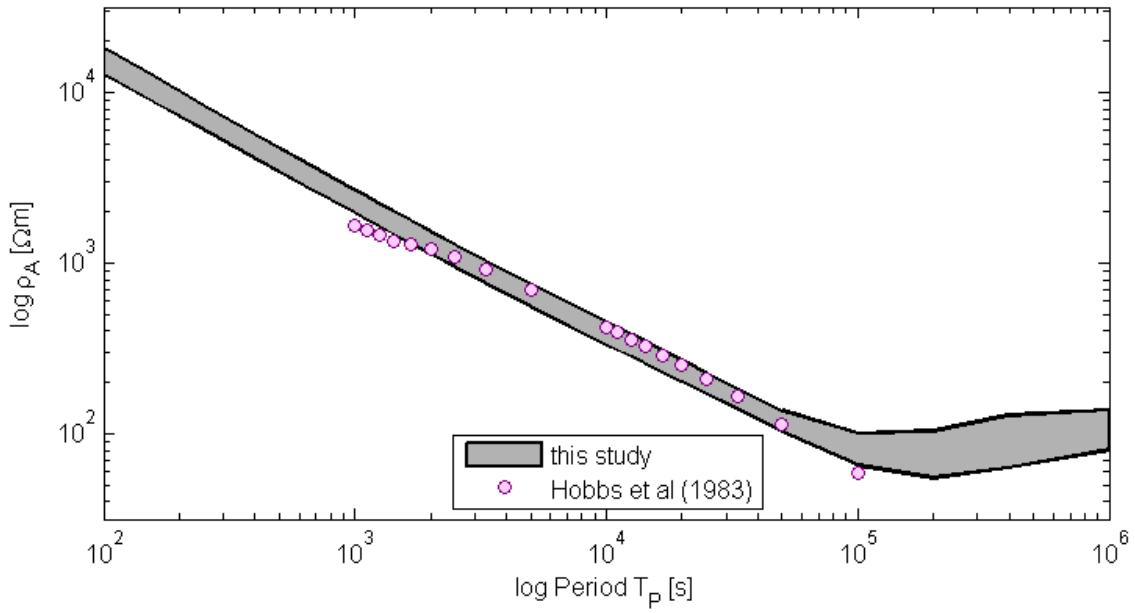

Figure 22: *The black/grey area are the upper and lower bounds for the apparent resistivity calculated in this study. The purple circles are calculated resistivities from the Apollo 15 magnetometer measurements by Hobbs et al (1983).*

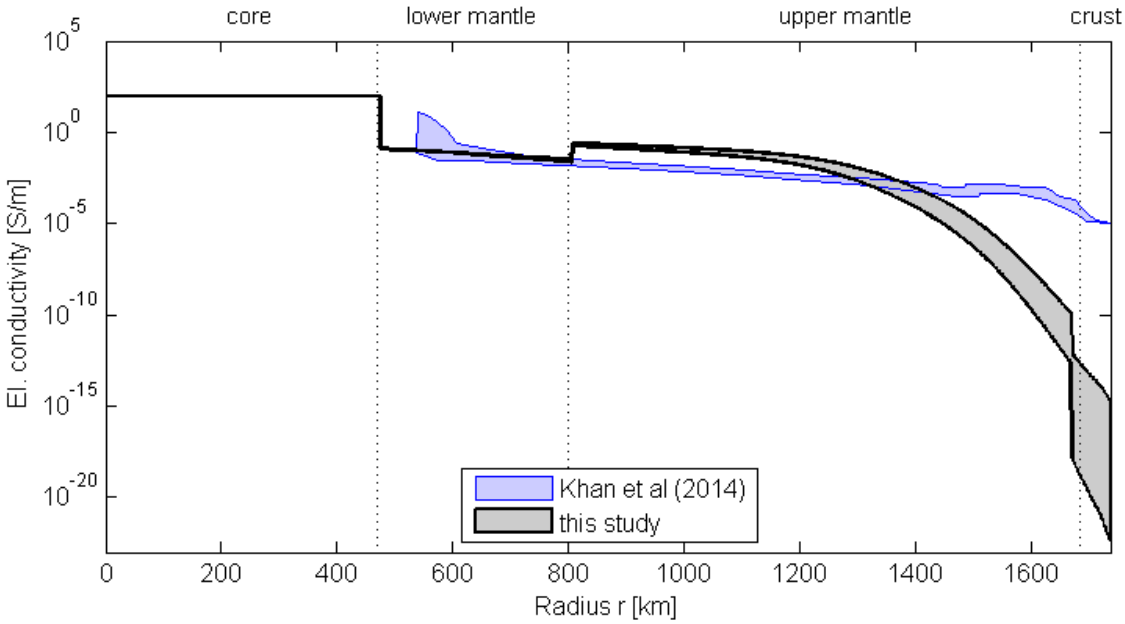

Figure 23: *Profile of electrical conductivity with upper and lower bounds from this study (black/gray) and from Khan et al (2014) (blue).*

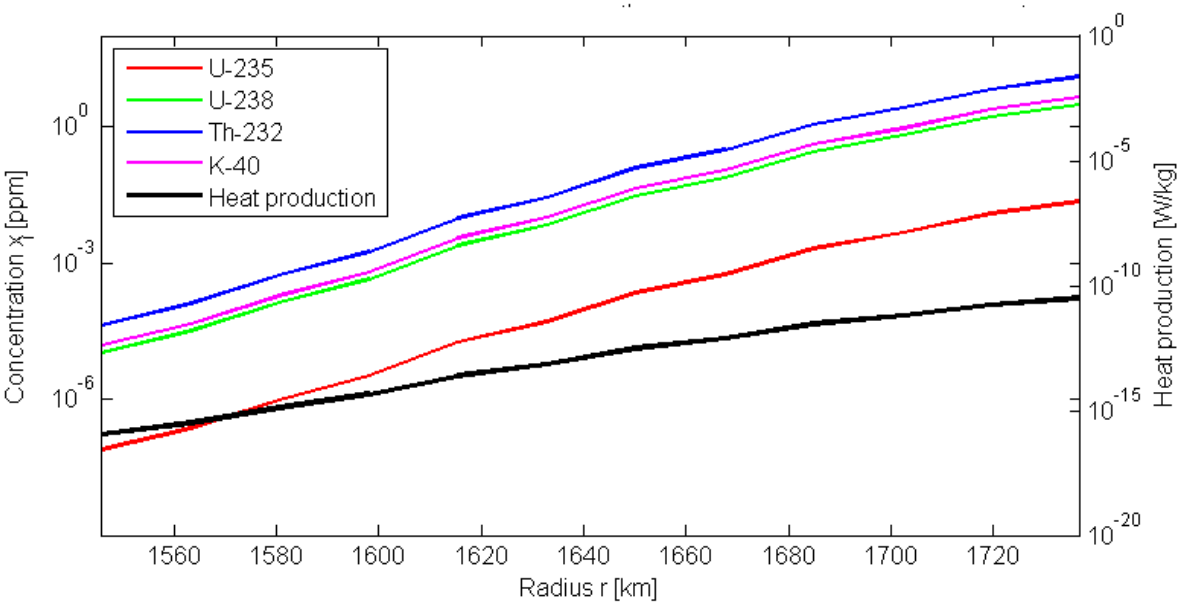

Figure 24: *Left axis: Concentration of radioactive elements versus radius (t = today). The ongoing crust formation leads to a depletion of the elements in the mantle and an enrichment in the crust. Right axis: Heat production by radioactive elements (t = today). The fractionation of the radioactive elements leads to strong heating in the crust.*

4 Discussion

4.1 Comparision to other results

The results of the here presented inversion procedure converged to a narrow parameter range. The initial temperature after differentiation could be constrained to 2910 ±40 K, the thickness of the lunar crust to 45 ±3 km, the depth of the inter-mantle boundary to 925 ±14 km, the core radius to 475 ±9 km and the water content of the lunar mantle minerals to 15 ±3 ppm. The lunar core is found to be completely frozen. Further the model results indicate two partially molten zones: One is located from the core-mantle boundary at r=475 km up to r=650 km with a melt fraction up to 30 % and the other from the inter-mantle boundary at r=800 km to r=1100 km with a melt fraction up to 27 %. The inversion results mostly confirm the previous studies about the lunar structure, but there are also contradictory results. Compared to the work of *Wieczorek (2009)* the crustal thickness and inter-mantle-boundary estimated in this work are in agreement. *Wieczorek (2009)* found the lunar crustal thickness on the day-side to be about 40-45 km, an inter-mantle-boundary at a depth of 900-1000 km and a lunar core to be <460 km. The discrepancy between the core radius found in this study to the one proposed by *Wieczorek (2009)* is relatively small and can be accounted to the different approach to constrain this parameter. The core radius in this study is found via the lunar mass, moment of inertia, magnetometer transfer-function and tidal deformation behaviour, whereas *Wieczorek (2009)* used only lunar seismometer data to determine it. A major disagreement between this study and *Wieczorek (2009)* is the state of the core. In this study the core is found to be completely solid, while *Wieczorek (2009)* proposes a solid inner and a liquid outer core. The selenotherm derived in this study is mostly in agreement with the mantle selenotherm found by *Kuskov & Kronrod (2009)*. In comparision to *Khan et al (2014)* the selenotherm found in this study is at least 200 K below. Further the temperature gradient in this study increases with depth in contrast to the work of *Khan et al (2014)*. This shape of the selenotherm is a result of

the Nu/Ra-relation used to mimick the mantle convection. Inside the (partial) molten zones of the mantle convection takes place and an effective thermal conductivity is high. This leads to a decrease of the temperature gradient in this partial molten domains close to adiabatic conditions. In the overlying zones heat can only be transported through conduction resulting in a decrease of the temperature gradient. The here presented seismic velocities show deviations to the velocities presented in the very preliminary lunar reference model (VPREMOON) by *Garcia et al (2014)*, to the model from *Khan et al (2014)* and to the model of *Kuskov et al (2014)* (Fig. 20 and 21). The two partially melted zones found in this study (Fig. 17) lead to a significant decrease in P- and S-wave velocities in this domains. Futhermore, the profiles for P- and S-wave velocities in this study are decreasing with depth in general. The effect of the temperature dependency of the elastic moduli (K and G decrease with higher temperatures) dominates over the pressure dependency of them (K and G increase with greater pressures). The modelled transfer function in a form of the frequency dependent apparent resistivities fits well the observed transfer function published by *Hobbs et al (1983)*. The calculated electrical conductivity profile (Fig. 23) is in agreement with the results from *Khan et al (2014)*, except the region in the upper mantle and in the crust. *Khan et al (2014)* propose much larger conductivity in this zones, possibly due to the different selenotherm (Fig. 15). Fig. 24 shows the concentration of radioactive isotopes and the related heat production as a function of depth. The calculated lunar gravitational acceleration (Fig. 18) is also in agreement with the observed acceleration on the lunar surface. This can be expected as the lunar mass was one of the fitted parameters. The water content of lunar minerals found in this study is around 15 ppm. This is consistent with the values provided by *Karato (2013)* who estimated the water content of 0.01 wt % for lunar minerals from both electrical conductivity and seismic wave attenuation. The surface heat flow of the model is about 6 mW/m2 which is lower than the average observed heat flow of 8 mW/m2. The reason therefore is the low thermal gradient of the model near the surface. The application of an insulating, porous layer of regolith with low thermal conductivity may lead to a steeper gradient and higher heat flux in the model.

4.2 Simplifications and neglected aspects

During the development of the models some simplifications and neglections were made. One point is, that the models were designed for the one-dimensional spherical case to save the computation time and to allow a great number of Downhill Simplex runs to be done. However, the nature of the moon is non-spherically three-dimensional which can be already observed by comparing the near-side with the far-side or the brighter and darker surface areas. Nethertheless, the one-dimensional approach seems to be legitimite as far as we assume that with an increasing depth the mineralogical heterogeneities and non-spherical character of mineralogical discontinuities are vanishing. Another point that could be further improved in the model are the fixed (not time-dependent) crust/mantle, inter-mantle and core-mantle boundaries during the model run. Convective processes, which were modelled by an effective thermal conductivity, not only transport heat but also may lead to a redistribution of minerals. This time-dependant mineralogy was not taken into account in the present study. Further, the melting of mantle and crustmay lead to some changes in the mineralogical composition profile.

5 Outlook

The here presented technique of a joint inversion of mass, moment of inertia, electrical and elastical properties of the Moon successfully converged to a narrow area of physical parameters by fitting the model to the observed data. With respect to some issues that could be further refined, the models also can be applied to other celestial bodies. Especially in the context of the current space missions "New Horizons" or "Cassini Huygens" the presented approach could bring new insights to the Galilean moons, asteroid belt objects and trans neptunian objects and provide some constraints to their interior structure.

6 Acknowledgements

First of all I want to thank Dr. Nikolai Bagdassarov for providing me the opportunity to work on the very interesting topic of the lunar evolution and structure, for discussing the results of this work and for giving inspirational clues for improvements. Further, a special thank to Dr. Harro Schmeling for letting me use his Downhill Simplex algorithm code for the inversion and for teaching me a lot of useful theoretical issues used in this study.

7 Bibliography

T.J. Ahrens, K.G. Holland, G.Q. Chen (2002)
Phase diagram of iron, revised-core temperatures. Geophysical Research Letters. doi: 10.1029/2001GL014350

L. Dai, S. Karato (2009)
Electrical conductivity of orthopyroxene: Implications for the water content of the asthenosphere. Proc. Jpn. Acad.,
Ser. B 85 (2009) Vol. 85, pp. 466-474

A. Duba, A.E. Ringwood (1972)
Electrical conductivity, internal temperatures and thermal evolution of the Moon. The Moon 7 (1973), pp. 356-376

T.S. Duffy, D.L. Anderson (1989)
Seismic Velocities in Mantle Minerals and the Mineralogy of the Upper Mantle. Journal of Geophysical Research, Vol. 95, No. B2. pp. 1895-1912

R.M. Fisher, G.P. Huffman, T. Nagata and F.C. Schwerer (1977)
Electrical Conductivity and the Thermocline of the Moon. Philosophical Transactions of the Royal Society of London. Series A, Mathematical and Physical Sciences, Vol. 285, No. 1327, The Moon: A New Appraisal from Space Missions and Laboratory Analyses (Mar. 31, 1977), pp. 517-521

R.F. Garcia, J. Gagnepain-Beyneix, S. Chevrot, P. Lognonné (2014)
Very preliminary reference Moon model. Elsevier Physics of the Earth and Planetary Interiors 188 (2011), pp. 96–113

R. Grimm (2013)
Geophysical constraints on the lunar Procellarum KREEP-terrane. Journal of Geophysical Research, Vol. 118, pp. 768-777, doi: 10.1029/2012JE004114

Y. Harada, S. Goossens, K. Matsumoto, J. Yan, J. Ping, H. Noda, J. Haruyama (2014)
Strong tidal heating in an ultralow-viscosity zone at the core-mantle boundary of the Moon. Nature Geoscience (2014), doi: 10.1038/NGEO2211

Z. Hashin, S. Shtrikman (1962)
A variational approach to the elastic behaviour of multiphase materials. J. Mech. Phys. Solids 11, pp. 127-140

B.A. Hobbs, L.L Hood, F. Herbert, C.P. Sonett (1983)
An upper bound on the radius of a highly electrically conducting lunar core. Journal of Geophysical Research (1983), Vol. 88, pp. B97-B102

Y. Iwase, S. Honda (1997)
An interpretation of the Nusselt-Rayleigh number relationship for convection in a spherical shell. Geophys. J. Int. (1997) 130, pp. 801-804

S. Karato (2013)
Geophysical constraints on the water content of the lunar mantle and its implications for the origin of the Moon. Elsevier Earth and Planetary Science Letters (2013), doi: 10.1016/j.epsl.2013.10.001

S. Karato and D. Wang (2013)
Electrical conductivity of minerals and rocks. Physics and Chemistry of the Deep Earth (2013), Wiley Online Library. doi: 10.1002/9781118529492.ch5

A. Khan, K. Mosegaard, J.G. Williams, P. Lognonne (2004)
Does the Moon possess a molten core? Probing the deep lunar interior using results from LLR and Lunar Prospector. Journal of Geophysical Research (2004), Vol. 109, E09007, doi: 10.1029/2004JE002294

A. Khan, J.A.D. Connolly, N. Olsen, K. Mosegaard (2006)
Constraining the composition and thermal state of the Moon from an inversion of electromagnetic lunar day-side transfer functions. Elsevier Earth and Planetary Science Letters 248 (2006), doi: 10.1016/j.epsl.2006.04.008

A. Khan, J.A.D. Connolly, A. Pommier, J. Noir (2014)
Geophysical evidence for melt in the deep lunar interior and implications for lunar evolution. American Geophysical Union 2014, doi: 10.1002/2014JE004661

O.L. Kuskov, V.A. Kronrod, E.V. Kronrod (2014)
Thermo-chemical constraints on the interior structure and composition of the lunar mantle. Elsevier Phyiscs of the Earth and Planetary Interiors 235 (2014), pp. 84-95, doi: 10.1016/j.pepi.2014.07.011

D. Leavy, T. Madden (1974)
Lunar electrical conductivity. Nature Vol. 250 (1974), pp.553-555

G.R. Olfoeft, A.L. Frisillo, D.W. Strangway, H. Sharpe (1973)
Temperature dependence of electrical conductivity and lunar temperatures. The Moon 9 (1973), pp. 79-87

E.C. Robertson (1988)
Thermal properties of rocks. United States Department of the Interior, USGS, Open-File Report 88-441

B. Romanowicz, A. Dziewonski (2007)
Treatise on Geophysics Vol. 1, pp. 667. ISBN 978-0-444-53459-0

R.N. Thompson, S.A. Gibson (2000)
Transient high temperatures in mantle plume heads inferred from magnesian olivines in Phanerozoic picrites. Nature 407, 502–506.

M. Wieczorek (2009)
The interior structure of the Moon: What does geophysics have to say? Elements, Vol. 5, pp. 35-40, doi: 10.2113/gselements.5.1.35

J.G. Williams, D.H. Boggs, J. T. Ratcliff and J.O. Dickey (2002)
Lunar Love numbers and the deep lunar interior. Lunar and Planetary Science XXXIII (2002)

J.G. Williams, D.H. Boggs, and J. T. Ratcliff (2012)
Lunar moment of inertia, Love number and core. 43rd Lunar and Planetary Science Conference (2012)

H. Zhang and C.Z. Zhang (2004)
The Q Values of the Galilean Satellites and their Tidal Contributions to the Deceleration of Jupiter's Rotation.
Chin. J. Astron. Astrophys. Vol. 4 (2004), No. 5, pp. 499–506

V.N. Zharkov (1986)
Interior Structure of the Earth and Planets. Page 114. ISBN 3-7186-0067-6.

Appendix A

In the following the numerical codes are listed.
Legend: Comments
Functions
External Data

downhillstart.m (Script)
(modified version from Prof. Dr. H. Schmeling)

```
% Downhill Simplex Inversion - 5 parameters
format shortE
clear all
close all

% definitions
 nparam = 5;           % No of parameters to invert
npoints = nparam+1;    % No of points in the parameter space
  alpha = 1.;          % parameter for reflexion
   beta = 0.9;         % parameter for contraction
  gamma = 2;           % parameter for expansion

% Parameter
   Tini0  = 2500;         % Initial temperature
   dTini0 = 100;
  dcrust0 = 50;   % Thickness of crust
 ddcrust0 = 10;
 dmantle0 = 750;          % Depth of lower/upper mantle boundary
ddmantle0 = 25;
   rcore0 = 200;       % Core radius
  drcore0 = 15;
      cw0 = 10;        % Water content of minerals
     dcw0 = 0.5;

   rangeS = 12;        % coarse variation (outer loop)
   range  = 0.07;      % fine variation (inner loop)
    ifin2 = 20;        % number of outer loops
     ifin = 30;        % number of inner loops

for irun2=1:1:ifin2
    if irun2>1
       Tini0 = Tini0*(1+(randi([(-rangeS) (rangeS)]))/100);
       dcrust0 = dcrust0*(1+(randi([(-rangeS) (rangeS)]))/100);
       cw0 = cw0*(1+(randi([(-rangeS) (rangeS)]))/100);
       dmantle0 = dmantle0*(1+(randi([(-rangeS) (rangeS)]))/100);
       rcore0 = rcore0*(1+(randi([(-rangeS) (rangeS)]))/100);
    end;
for irun=1:ifin

q = irun

    Tini = Tini0*(1+range*(rand-0.5));
   dTini = dTini0*(1+range*(rand-0.5));
  dcrust = dcrust0*(1+range*(rand-0.5));
 ddcrust = ddcrust0*(1+range*(rand-0.5));
 dmantle = dmantle0*(1+range*(rand-0.5));
```

```
ddmantle = ddmantle0*(1+range*(rand-0.5));
   rcore = rcore0*(1+range*(rand-0.5));
  drcore = drcore0*(1+range*(rand-0.5));
      cw = cw0*(1+range*(rand-0.5));
     dcw = dcw0*(1+range*(rand-0.5));

% Starting parameters, they should not be equal 0!
P0(1,:) =           [ Tini, dcrust, dmantle, rcore, cw];
P0(2,:) = P0(1,:) + [dTini,      0,       0,     0,  0];
P0(3,:) = P0(1,:) + [    0,ddcrust,       0,     0,  0];
P0(4,:) = P0(1,:) + [    0,      0,ddmantle,     0,  0];
P0(5,:) = P0(1,:) + [    0,      0,       0,drcore,  0];
P0(6,:) = P0(1,:) + [    0,      0,       0,     0,dcw];

% Termination parameters
    eps = 0.01;     % Misfit better than eps
epsconv = 1e-6;     % Difference between subsequent norm of all normalized parameters
   nmax = 1000;     % Maximum iterations

%Initializing several parameters
       ii = 0;
icompress = 1;
   P0last = 999;
converged = 0;

% Initial misfit
for i=1:npoints
    mf(i) = 1e6;
end

% Downhill loop starts
while min(mf) > eps && ii < nmax && converged == 0

% Misfit of new points in parameter space
if icompress == 1
   for i=1:npoints
      [mf(i),P0(i,:),mall]=inv_start(P0(i,:));
   end
end
icompress = 0;

% which has the worst, best fit?
[C,imax]=max(mf);
[C,ibest]=min(mf);

% which has the second worst fit?
mfreduced=mf;
mfreduced(imax)=[];
[C,imax2]=max(mfreduced);

% Centre of all points excluding the worst point
Pcentre=(sum(P0(:,:))-P0(imax,:))/(npoints-1);



% Mirror the worst point w.r.t centre
Pmir=Pcentre+(Pcentre-P0(imax,:))*alpha;

```

```
% Misfit of mirrored point
[mfmir,Pmir,mall]=inv_start(Pmir);


% Reflected point better than all others?
if mfmir < min(mf)
    % expand mirrired point
    Pmirexp=Pcentre+(Pcentre-P0(imax,:))*gamma;
    [mfmirexp,Pmirexp,mall]=inv_start(Pmirexp);
    % if better this is the new point, else dont expand, take the mirrored point as new point
    if mfmirexp < mfmir
        Pnew = Pmirexp;
        mfnew = mfmirexp;
        dhcontrol='expanded, wrst pt --> best';
    else
        Pnew = Pmir;
        mfnew = mfmir;
        dhcontrol='reflected, wrst pt --> best';
    end
% Reflected point better than second worst point? Then this is still the new point
elseif mfmir < mf(imax2)
    Pnew = Pmir;
    mfnew = mfmir;
    dhcontrol='reflected2nd, wrst pt --> better';
else
    % Contraction: first define worst point, either old worst or reflected
    Pwrst = P0(imax,:);
    if mfmir < mf(imax)
       Pwrst = Pmir;
    end
    % Contraction; Move worst point to half way towards centre point
    Pwrst = Pwrst+(Pcentre-Pwrst)*beta;
    [mfPwrst,Pwrst,mall] = inv_start(Pwrst);
    % if this improves its fit use it and start with it as new point
    if mfPwrst < mf(imax)
        Pnew = Pwrst;
        mfnew = mfPwrst;
        dhcontrol='contract wrst pt';
    else
        % Compression: Move all points half way towards the best point
        icompress = 1;
        for i = 1:npoints
            P(i,:) = (P0(i,:)+P0(ibest,:))/2;
        end
        dhcontrol='compress simplex';
    end
end

% Write the new points (either only Pnew or the compressed points) to P0
if icompress == 0
    % The other points are kept, only the worst is improved
    P0(imax,:)=Pnew;
    mf(imax) = mfnew;
else
    % All points compressed towards the best point
    P0=P;
end
% Output and termination?
diff=(norm(P0)-P0last)/P0last;
```

```
P0last=norm(P0);
disp([num2str([irun  ii]) ' ' num2str(mf(ibest)) ' , ' num2str(P0(ibest,:)) ' , ' num2str(diff) ', '
dhcontrol])
disp(' ')
ii = ii+1;


if abs(diff) < epsconv
    converged = 1
end
end

[mffinal,P0(ibest,:),mall] = inv_start(P0(ibest,:));
Pfin(((irun2-1)*ifin+irun),:) = [P0(ibest,:),mffinal,mall];
dlmwrite('P.txt',Pfin);
end
end;
disp('Pfin and misfit')
disp(Pfin)

```

inv_start.m (Function)

```
function [misfit,P,misfall] = inv_start(P)
% Function to start the models
%-----------------------------------------------------------------
  steps = 101;                % model resolution
      R = 1737000;            % lunar radius
      r = linspace(0,R,steps);
     dr = ceil((r(2)-r(1))/1000);
     Rm = R/1000;
if P(1) < 1800       ; P(1) = 1800      ;end
if P(1) > 3800       ; P(1) = 3800      ;end
if P(2) < 2*dr       ; P(2) = 2*dr      ;end
if P(2) >100         ; P(2) = 100       ;end
if P(4) < 2*dr       ; P(4) = 2*dr      ;end
if P(4) > 400        ; P(4) = 400       ;end
if P(3) < P(2)+2*dr  ; P(3) = P(2)+2*dr ;end
if P(3) > Rm-P(4)-2*dr;P(3)=Rm-P(4)-2*dr;end
if P(5) < 0.1        ; P(5) = 0.1       ;end
if P(5) > 50         ; P(5) = 50        ;end

   Tini = P(1);    dcrust = P(2);     dmantle = P(3);
  rcore = P(4);        cw = P(5);

     rx = [dcrust*1000,dmantle*1000,R-rcore*1000];
     Tp = load('mt_periods.txt')';
     Tp = 10.^Tp;
      N = size(Tp,2);

% Models
[VARa,VARb,VARc,VARd] = sel_start(Tini,rx,r,R,steps);
  [Tf1,Tf2,HShi,HSlo] = mt_start(steps,rx,VARa(2,:),cw,Tp,N);
               [k2,Q] = tid_start(steps,R,VARa(1,:),VARa(2,:),VARa(7,:),VARa(6,:),VARa(15:16,:),...
                                  ...VARc,cw,VARa(17,:));
        [m1,m2,m3,m4] = inv_misfit(VARc,Tf1,Tf2,k2);
               misfit = m1+m2+m3+m4;
             misfall = [m1,m2,m3,m4];
```

inv_misfit.m (Function)

```
function [m1,m2,m3,m4] = inv_misfit(VARc,Tf1,Tf2,k2)
% Function to calculate the misfit
%--------------------------------------------------------------
 Mlit = 7.34767309*10^22;              % Reference mass
 Ilit = 0.3928;                        % Reference intertia
k2lit = 0.024;                         % Reference k2
   tf = load('mt_transferfunction.txt');
   tp = tf(:,1);
 rhoa = tf(:,2);
    N = size(tp,1);
  Tf1l = log10(Tf1);
  Tf2l = log10(Tf2);
   Tfa = (Tf1l+Tf2l)/2;
 rhoal = log10(rhoa);
 for i=1:1:N
     mfa(i) = sqrt((rhoal(i)-Tfa(i+5)).^2)/rhoal(i);
 end;
m1 = sqrt((VARc(1)-Mlit)^2)/Mlit;
m2 = sqrt((VARc(2)-Ilit)^2)/Ilit;
m3 = sum(mfa)/N;
m4 = sqrt((k2-k2lit)^2)/k2lit;
```

sel_start.m (Function)

```
function [VARa,VARb,VARc,phase] = sel_start(Tini,rx,r,R,steps)
% Function containing the thermal evolution model
%--------------------------------------------------------------
 tmax = 4400;                                % model runtime
 Ma2s = 60*60*24*365*10^6;                   % Ma in seconds conversion
 tmax = tmax*Ma2s;
 Tsur = 273;                                 % surface temperature
   rx = R-rx;
   dr = r(2)-r(1);
    t = 0;
    P = (-1.59*(r*10^-6).^2+4.798)*10^9;     % initial pressure estimation
    g = linspace(0,1.6,steps);               %    "    gravity      "
phase = [0,0,0,0,0,0,0,0];
   pr = zeros(1,steps);
 rho0 = load('sel_rho0.txt');                % density raw-data
alpha = load('sel_alpha.txt');               % thermal expansivity data
modul = load('sel_kmodul.txt');              % elastic modulus and derivatives (P,T) data

 [s,up,lo,cmb] = sel_composition(r,rx,steps);
             T = sel_adiabat(Tini,g,s,cmb,dr);
[Kt,K,G,K2,G2] = sel_elasticity(s,T,P,modul,phase,pr,up,lo,cmb,steps,0);
           rho = sel_density(s,P,T,alpha,rho0,Kt,steps);
            cp = sel_heatcapacity(s,P,T,steps,lo,cmb);
[lam,phase,pr] = sel_heatconductivity(T,P,g,cp,lo,cmb,dr,steps);
  [g,M,I,P,mr] = sel_gravity(rho,r,dr,steps);
    [H,C,Hdat] = sel_radiodistribution(mr,0,cmb,0,0,0,tmax,steps);
             k = lam./(rho.*cp);             % heat diffusivity
          kmax = max(k);                     % max. value of k
            dt = round(dr^2/(2*kmax)*0.25);  % max. size of timestep
         icalc = 10;  Icalc = 10;            % parameter calculation timestepping
         jcalc = 2;   Jcalc = 2;
```

```
      T(steps) = Tsur;
          VARb = [cmb,lo,up,Ma2s,steps,R,Tsur,Tini];
while t<=tmax                                  % Time loop start
      t = t+dt;
    for i=2:1:steps-1
        Tnew(i-1) = T(i)+dt*(((k(i+1)+k(i))/2)*((r(i+1)+r(i))/2)^2*(T(i+1)-T(i))-((k(i-1)+k(i))/2)*...
                    ...((r(i-1)+r(i))/2)^2*(T(i)-T(i-1)))/(r(i)^2*dr^2)+dt*H(i)/cp(i);
    end;
     T(2:steps-1) = Tnew;
             T(1) = T(2);
    if jcalc>Jcalc
       [H,C,Hdat] = sel_radiodistribution(mr,phase(6),cmb,C,Hdat,t,tmax,steps);
               cp = sel_heatcapacity(s,P,T,steps,lo,cmb);
   [lam,phase,pr] = sel_heatconductivity(T,P,g,cp,lo,cmb,dr,steps);
                k = lam./(rho.*cp);
             kmax = max(k);
               dt = round(dr^2/(2*kmax)*0.9);
            jcalc = 1;
    end;
    if icalc>Icalc
   [Kt,K,G,K2,G2] = sel_elasticity(s,T,P,modul,phase,pr,up,lo,cmb,steps,0);
              rho = sel_density(s,P,T,alpha,rho0,Kt,steps);
        [g,M,I,P] = sel_gravity(rho,r,dr,steps);
            icalc = 1;
    end;
        icalc = icalc+1;
        jcalc = jcalc+1;
end;
[Kt,K,G,K2,G2] = sel_elasticity(s,T,P,modul,phase,pr,up,lo,cmb,steps,1);
VARa = [r;T;lam;rho;cp;g;P;H;C;K;K2;G;G2;pr];
VARc = [M,I,up,lo,cmb,t];
```

sel_adiabat.m (Function)

```
function T = sel_adiabat(Tini,g,s,cmb,dr)
% Function to calculate the adiabate
%-----------------------------------------------------------------
load sel_alpha.txt;
    T = zeros(1,size(s,1));
 T(1) = Tini;
alpha = zeros(1,size(s,1));
    a = sel_alpha;
for i=1:1:size(s,1);
    if i<=cmb
    cp(i) = 1200;
   rho(i) = 3000;
    else
    cp(i) = 600;
   rho(i) = 6000;
    end;
end;
for i=1:1:size(s,1)-1
    alpha(i) = (s(i,1)*(s(i,2)*a(2)+s(i,3)*a(3))+s(i,4)*(s(i,5)*a(5)+s(i,6)*a(6))...
               ...+s(i,7)*(s(i,8)*a(8)+s(i,9)*a(9))+s(i,10)*(s(i,11)*a(11)+s(i,12)*a(12)...
               ...+s(i,13)*a(13))+s(i,14)*(s(i,15)*a(15)+s(i,16)*a(16)+s(i,17)*a(17))...
               ...+s(i,18)*(s(i,19)*a(19)+s(i,20)*a(20)+s(i,21)*a(21)+s(i,22)*a(22))...
               ...+s(i,23)*(s(i,24)*a(24)+s(i,25)*a(25))+s(i,26)*(s(i,27)*a(27)))/100;
```

```
    dT = alpha(i)*g(i)*T(i)*dr/cp(i);
    T(i+1) = T(i)+dT;
end;
T = fliplr(T);
```

sel_composition.m (Function)

```
function [s,up,lo,cmb] = sel_composition(r,rx,steps)
% Function to initialize the mineralogical composition
%-----------------------------------------------------------------
s0 = load('sel_min.txt');
for i=1:1:steps
    if r(i)<=rx(3)
       s(i,:) = s0(4,:);
       cmb = i;
    end;
    if r(i)>rx(3) && r(i)<=rx(2)
       s(i,:) = s0(3,:);
       lo = i;
    end;
    if r(i)>rx(2) && r(i)<=rx(1)
       s(i,:) = s0(2,:);
       up = i;
    end;
    if r(i)>rx(1)
       s(i,:) = s0(1,:);
    end;
end;
```

sel_density.m (Function)

```
function rho = sel_density(s,P,T,a,r0,Kt,steps)
% Function to link density(P,T) to mineralogy
%-----------------------------------------------------------------
T0 = 273.15;
dT = T-T0;
for i=1:1:steps
    rol(i) = s(i,2)*(r0(2)*(1-a(2)*dT(i))*(1+P(i)/Kt(i,1))) + s(i,3)*(r0(3)*...
        ...(1-a(3)*dT(i))*(1+P(i)/Kt(i,1)));
    rfs(i) = s(i,5)*(r0(5)*1/(1-a(5)*(T(i)-T0)+20*a(5)*(sqrt(T(i))-sqrt(T0)))) + ...
        ...s(i,6)*(r0(6)*1/(1-a(6)*(T(i)-T0)+20*a(6)*(sqrt(T(i))-sqrt(T0))));
    rsp(i) = s(i,8)*(r0(8)*(1-a(8)*dT(i))*(1+P(i)/Kt(i,7))) + s(i,9)*(r0(9)*...
        ...(1-a(9)*dT(i))*(1+P(i)/Kt(i,7)));
    rgt(i) = s(i,11)*(r0(11)*(1-a(11)*dT(i))*(1+P(i)/Kt(i,10))) + s(i,12)*(r0(12)*...
        ...(1-a(12)*dT(i))*(1+P(i)/Kt(i,10))) + s(i,13)*(r0(13)*(1-a(13)*dT(i))*(1+P(i)/Kt(i,10)));
    rop(i) = s(i,15)*(r0(15)*(1-a(15)*dT(i))*(1+P(i)/Kt(i,14))) + s(i,16)*(r0(16)*...
        ...(1-a(16)*dT(i))*(1+P(i)/Kt(i,14))) + s(i,17)*(r0(16)*(1-a(16)*dT(i))*(1+P(i)/Kt(i,14)));
    rcp(i) = s(i,19)*(r0(19)*(1-a(19)*dT(i))*(1+P(i)/Kt(i,18))) + s(i,20)*(r0(20)*...
        ...(1-a(20)*dT(i))*(1+P(i)/Kt(i,18))) + s(i,21)*(r0(21)*(1-a(21)*dT(i))*(1+P(i)/Kt(i,18)))...
        ... + s(i,22)*(r0(22)*(1-a(22)*dT(i))*(1+P(i)/Kt(i,18)));
    rti(i) = s(i,24)*(r0(24)*(1-a(24)*dT(i))*(1+P(i)/Kt(i,23))) + s(i,25)*(r0(25)*...
        ...(1-a(25)*dT(i))*(1+P(i)/Kt(i,23)));
    rfe(i) = s(i,27)*(r0(27)*(1-a(27)*dT(i))*(1+P(i)/Kt(i,26)));
    rho(i) = (rol(i)*s(i,1)+rfs(i)*s(i,4)+rsp(i)*s(i,7)+rgt(i)*s(i,10)+rop(i)*s(i,14)+...
        ...rcp(i)*s(i,18)+rti(i)*s(i,23)+rfe(i)*s(i,26))*10;
end;
```

sel_elasticity.m (Function)

```
function [Kt,Kup,Gup,Klo,Glo] = sel_elasticity(S,T,P,k,phase,part,up,lo,cmb,steps,q)
% Function to link shear- and bulk-modulus(P,T) to mineralogy
%-----------------------------------------------------------------

for i=1:1:steps
      Kol(i) = ((k(1,1)-k(2,1)*T(i))*10^9+k(3,1)*P(i));
      Gol(i) = ((k(4,1)-k(5,1)*T(i))*10^9+k(6,1)*P(i));

      Kpl(i) = ((k(1,4)-k(2,4)*T(i))*10^9+k(3,4)*P(i));
      Gpl(i) = ((k(4,4)-k(5,4)*T(i))*10^9+k(6,4)*P(i));

      Ksp(i) = ((k(1,7)-k(2,7)*T(i))*10^9+k(3,7)*P(i));
      Gsp(i) = ((k(4,7)-k(5,7)*T(i))*10^9+k(6,7)*P(i));

      Kgt(i) = ((k(1,10)-k(2,10)*T(i))*10^9+k(3,10)*P(i));
      Ggt(i) = ((k(4,10)-k(5,10)*T(i))*10^9+k(6,10)*P(i));

      Kop(i) = ((k(1,14)-k(2,14)*T(i))*10^9+k(3,14)*P(i));
      Gop(i) = ((k(4,14)-k(5,14)*T(i))*10^9+k(6,14)*P(i));

      Kcp(i) = ((k(1,18)-k(2,18)*T(i))*10^9+k(3,18)*P(i));
      Gcp(i) = ((k(4,18)-k(5,18)*T(i))*10^9+k(6,18)*P(i));

      Kti(i) = ((k(1,23)-k(2,23)*T(i))*10^9+k(3,23)*P(i));
      Gti(i) = ((k(4,23)-k(5,23)*T(i))*10^9+k(6,23)*P(i));

      Kfe(i) = k(1,26)*10^9;
      Gfe(i) = k(4,26)*10^9;
end;
S = S/100;
o = zeros(steps,1);
Kt = [Kol',o,o,Kpl',o,o,Ksp',o,o,Kgt',o,o,o,Kop',o,o,o,Kcp',o,o,o,o,Kti',o,o,Kfe',o];
if q==1
for i=steps:-1:up
    Kup(i) = 1/(S(i,4)/(Kpl(i)+4/3*Gti(i))+S(i,14)/(Kop(i)+4/3*Gti(i))+S(i,23)/...
        ...(Kti(i)+4/3*Gti(i)))-4/3*Gti(i);
    Klo(i) = 1/(S(i,4)/(Kpl(i)+4/3*Gpl(i))+S(i,14)/(Kop(i)+4/3*Gpl(i))+S(i,23)/...
        ...(Kti(i)+4/3*Gpl(i)))-4/3*Gpl(i);
    zup(i) = Gti(i)/6*(9*Kti(i)+8*Gti(i))/(Kti(i)+2*Gti(i));
    Gup(i) = 1/(S(i,4)/(Gpl(i)+zup(i))+S(i,14)/(Gop(i)+zup(i))+S(i,23)/(Gti(i)+zup(i)))-zup(i);
    zlo(i) = Gpl(i)/6*(9*Kpl(i)+8*Gpl(i))/(Kpl(i)+2*Gpl(i));
    Glo(i) = 1/(S(i,4)/(Gpl(i)+zlo(i))+S(i,14)/(Gop(i)+zlo(i))+S(i,23)/(Gti(i)+zlo(i)))-zlo(i);
end;

for i=up:-1:lo
    Kup(i) = 1/(S(i,1)/(Kol(i)+4/3*Gsp(i))+S(i,7)/(Ksp(i)+4/3*Gsp(i))+S(i,14)/(Kop(i)+4/3*Gsp(i))...
        ...+S(i,18)/(Kcp(i)+4/3*Gsp(i))+S(i,23)/(Kti(i)+4/3*Gsp(i)))-4/3*Gsp(i);
    Klo(i) = 1/(S(i,1)/(Kol(i)+4/3*Gop(i))+S(i,7)/(Ksp(i)+4/3*Gop(i))+S(i,14)/(Kop(i)+4/3*Gop(i))...
        ...+S(i,18)/(Kcp(i)+4/3*Gop(i))+S(i,23)/(Kti(i)+4/3*Gop(i)))-4/3*Gop(i);
    zup(i) = Gsp(i)/6*(9*Ksp(i)+8*Gsp(i))/(Ksp(i)+2*Gsp(i));
    Gup(i) = 1/(S(i,1)/(Gol(i)+zup(i))+S(i,7)/(Gsp(i)+zup(i))+S(i,14)/(Gop(i)+zup(i))+S(i,18)/...
        ...(Gcp(i)+zup(i))+S(i,23)/(Gti(i)+zup(i)))-zup(i);
    zlo(i) = Gop(i)/6*(9*Kol(i)+8*Gop(i))/(Kol(i)+2*Gop(i));
    Glo(i) = 1/(S(i,1)/(Gol(i)+zlo(i))+S(i,7)/(Gsp(i)+zlo(i))+S(i,14)/(Gop(i)+zlo(i))+S(i,18)/...
        ...(Gcp(i)+zlo(i))+S(i,23)/(Gti(i)+zlo(i)))-zlo(i);
end;
```

```
for i=lo:-1:cmb
    Kup(i) = 1/(S(i,1)/(Kol(i)+4/3*Ggt(i))+S(i,10)/(Kgt(i)+4/3*Ggt(i))+S(i,14)/(Kop(i)+4/3*Ggt(i))...
        ...+S(i,18)/(Kcp(i)+4/3*Ggt(i))+S(i,23)/(Kti(i)+4/3*Ggt(i)))-4/3*Ggt(i);
    Klo(i) = 1/(S(i,1)/(Kol(i)+4/3*Gop(i))+S(i,10)/(Kgt(i)+4/3*Gop(i))+S(i,14)/(Kop(i)+4/3*Gop(i))...
        ...+S(i,18)/(Kcp(i)+4/3*Gop(i))+S(i,23)/(Kti(i)+4/3*Gop(i)))-4/3*Gop(i);
    zup(i) = Ggt(i)/6*(9*Kgt(i)+8*Ggt(i))/(Kgt(i)+2*Ggt(i));
    Gup(i) = 1/(S(i,1)/(Gol(i)+zup(i))+S(i,10)/(Ggt(i)+zup(i))+S(i,14)/(Gop(i)+zup(i))+S(i,18)/...
        ...(Gcp(i)+zup(i))+S(i,23)/(Gti(i)+zup(i)))-zup(i);
    zlo(i) = Gop(i)/6*(9*Kol(i)+8*Gop(i))/(Kol(i)+2*Gop(i));
    Glo(i) = 1/(S(i,1)/(Gol(i)+zlo(i))+S(i,10)/(Ggt(i)+zlo(i))+S(i,14)/(Gop(i)+zlo(i))+S(i,18)/...
        ...(Gcp(i)+zlo(i))+S(i,23)/(Gti(i)+zlo(i)))-zlo(i);
end;

for i=cmb:-1:1
    Kup(i) = Kfe(i);
    Klo(i) = Kfe(i);
    Gup(i) = Gfe(i);
    Glo(i) = Gfe(i);
end;
if phase(2)>0
for i=phase(2):1:phase(3)
    Gup(i) = Gup(i)+part(i)/(1/(-Gup(i))+(2*(1-part(i))*(Kup(i)+2*Gup(i)))/(5*Gup(i)*(Kup(i)+...
        ...4/3*Gup(i))));
    Glo(i) = (1-part(i))/(1/(Gup(i))+(2*(part(i))*Klo(i))/(5*Gup(i)*Kup(i)));
end;
end;
if phase(4)>0
for i=phase(4):1:phase(5)
    Gup(i) = Gup(i)+part(i)/(1/(-Gup(i))+(2*(1-part(i))*(Kup(i)+2*Gup(i)))/(5*Gup(i)*(Kup(i)+...
        ...4/3*Gup(i))));
    Glo(i) = (1-part(i))/(1/(Gup(i))+(2*(part(i))*Klo(i))/(5*Gup(i)*Kup(i)));
end;
end;
if phase(6)>0
for i=phase(6):1:phase(7)
    Gup(i) = 0;
    Glo(i) = 0;
end;
end;
else
Gup = 0; Kup = 0; Glo = 0; Klo = 0;
end;
```

sel_gravity.m (Function)

```
function [g,M,I,P,mr] = sel_gravity(rho,r,dr,steps)
% Function to calculate gravitation acceleration, masss, pressure and interia
%--------------------------------------------------------------------------
    G = 6.67384*10^-11;
    g = zeros(1,steps);
    P = zeros(1,steps);
   mr = zeros(1,steps);
    m = 4/3*pi*r(1)^3*rho(1);
    j = 0;
mr(1) = m;
for i=2:1:steps
    g(i) = G*m/r(i)^2;
```

```
   mr(i) = 4/3*pi*(r(i)^3-r(i-1)^3)*rho(i);
       m = m+mr(i);
       j = j+8/15*pi*(r(i)^5-r(i-1)^5)*rho(i);
end;
for i=steps-1:-1:1
    P(i) = P(i+1)+(rho(i+1)+rho(i))/2*g(i)*dr;
end;
M = m;
I = j/(M*r(steps)^2);
```

sel_heatcapacity.m (Function)

```
function cp = sel_heatcapacity(S,P,T,steps,lo,cmb)
% Function to calculate (eff.) heat capacity
%-----------------------------------------------------------------
Ti = linspace(1,4000,4000);
cpol = (87.36+0.08717.*Ti-3.699e6.*Ti.^-2+843.6.*Ti.^(-0.5)-2.237e-5.*Ti.^2)/0.1407;
cppx = (264.8+9.46e-4.*Ti-12.958e6.*Ti.^-2)/0.21655;
cpfe = 700;
Lfe = 2*10^5;
Lpx = 4*10^5;
Lpe = 4*10^5;
[PPx,PPe,PFe] = sel_phase(P,steps);
for i=1:1:steps
      tot = S(i,1)+S(i,14)+S(i,18)+S(i,26);
    cp(i) = S(i,1)/tot*cpol(round(T(i)))+(S(i,14)+S(i,18))/tot*cppx(round(T(i)))+S(i,26)/tot*cpfe;
if i<cmb
if T(i)>=PFe(i)-10 && T(i)<=PFe(i)+10;
   cp(i) = cp(i)+Lpe/20;
end;
end;
if i>=cmb && i<lo
if T(i)>=PPe(1,i) && T(i)<=PPe(2,i);
   cp(i) = cp(i)+Lpe/(PPe(2,i)-PPe(1,i));
end;
end;
if i>=lo
if T(i)>=PPx(1,i) && T(i)<=PPx(2,i);
   cp(i) = cp(i)+Lpx/(PPx(2,i)-PPx(1,i));
end;
end;
end;
```

sel_heatconductivity.m (Function)

```
function [lam,phase,part] = sel_heatconductivity(T,P,g,cp,lo,cmb,dr,steps)
% Function to calculate (eff.) heat conductivity and melt fraction
%-----------------------------------------------------------------
  [PPx,PPe,PFe] = sel_phase(P,steps);
              A = 0.73;
              B = 1293;
              C = 0.034*10^-9;
           lam0 = (A+B./(77+T)).*(exp(C*P));% Wärmeleitfähigkeit Mantel, Gradient mit der Tiefe
           lamc = 0.001;                    % Temperaturkoeff. der Wärmeleitfähigkeit
    lam0(1:cmb) = 50;                       % Wärmeleitfähigkeit Eisen
```

```
        lammax = 150;                       % max. conductivity (numerical reasons)
           aMa = 2.1;                       % Koeffizient Mantel
           bMa = 0.2;                       % Exponent Mantel
1975       RacMa = 1296;                    % kritische Rayleighzahl Mantel
     threshold = 0.3;
        alphaM = 2.8*10^-5;
          rhoM = 3300;
part = zeros(1,steps);      bot = zeros(1,3);         top = zeros(1,3);
1980
for i=1:1:cmb
    if T(i)>PFe(i)        part(i) = 1;
    if bot(1)==0           bot(1) = i;
    end;
1985    top(1) = i;
    lam0(i) = lammax;
    end;
end;
for i=cmb+1:1:lo
1990    if T(i)>=PPe(1,i)     part(i) = (T(i)-PPe(1,i))/(PPe(2,i)-PPe(1,i));
    if bot(2)==0           bot(2) = i;
    end;
    top(2) = i;
    end;
1995    if part(i)>1          part(i) = 1;
    end;
end;
for i=lo+1:1:steps
    if T(i)>=PPx(1,i)     part(i) = (T(i)-PPx(1,i))/(PPx(2,i)-PPx(1,i));
2000    if bot(3)==0           bot(3) = i;
    end;
    top(3) = i;
    end;
    if part(i)>1          part(i) = 1;
2005    end;
end;
lam = lam0;
f = [0,0];
n=0;
2010 if bot(3)>0                            % Nusselt-Zahl oberer Mantel
   for i=bot(3):1:top(3)
   f(1) = f(1)+part(i);
      n = n+1;
   end;
2015   f(1) = f(1)/n;
   mid1 = round((bot(3)+top(3))/2);
   etaM = 10^18;
    Ra1 = g(mid1)*alphaM*rhoM^2*cp(mid1)*(T(bot(3))-T(top(3)))*(abs(bot(3)-top(3))*dr)^3/(5*etaM);
    Nu1 = aMa*(abs(Ra1/RacMa))^bMa;
2020    if f(1)<threshold
    Nu1 = Nu1*(f(1)/threshold)^2;
    end;
   if Nu1<1
      Nu1 = 1;
2025   end;
   for i=bot(3):1:top(3)
 lam(i) = lam0(i)*Nu1;
   end;
else
2030    Nu1 = 1;
```

```
end;
n=0;
if bot(2)>0                              % Nusselt-Zahl oberer Mantel
   for i=bot(2):1:top(2)
   f(2) = f(2)+part(i);
      n = n+1;
   end;
   f(2) = f(2)/n;
   mid2 = round((bot(2)+top(2))/2);
   etaM = 10^18;
    Ra2 = g(mid2)*alphaM*rhoM^2*cp(mid2)*(T(bot(2))-T(top(2)))*(abs(bot(2)-top(2))*dr)^3/(3*etaM);
    Nu2 = aMa*(abs(Ra2/RacMa))^bMa;
   if f(2)<threshold
    Nu2 = Nu2*(f(2)/threshold)^3;
   end;
   if Nu2<1
      Nu2 = 1;
   end;
   for i=bot(2):1:top(2)
 lam(i) = lam0(i)*Nu2;
   end;
else
    Nu2 = 1;
end;
phase = [0,top(1),bot(1),top(2),bot(2),top(3),bot(3),Nu1,Nu2];
```

sel_phase.m (Function)

```
function [PhasePx,PhasePe,PhaseFe] = sel_phase(P,steps)
% Function containing the phase-diagramm for mantle/core
%-----------------------------------------------------------------
 GPa = 10^9;
for i=1:1:steps
        if P<2.25*GPa
        PhasePe(2,i) = 1700+77.8/(GPa)*P(i);
        else
        PhasePe(2,i) = 1780+42.14/(GPa)*P(i);
        end;
        if P<2.5*GPa
        PhasePe(1,i) = 1150+108/(GPa)*P(i);
        else
        if P<3.7*GPa
        PhasePe(1,i) = 1000+162.16/(GPa)*P(i);
        else
        PhasePe(1,i) = 1275+89.75/(GPa)*P(i);
        end;
        end;

        PhasePx(2,i) = 1153+150/GPa*P(i);
        PhasePx(1,i) = 1073+106.7/GPa*P(i);

        PhaseFe = 800/(17*10^9)*P+1800;
end;
```

sel_radiodistribution.m (Function)

```
function [H,C,Hdat] = sel_radiodistribution(m,bot,cmb,C,Hdat,t,tmax,steps)
% Function to calculate heat production and distribute rad. elements
%-----------------------------------------------------------------
Ga2s = 3600*24*365*10^9;
D = 15;
ppm = 10^-6;
  %  Oberflächenkonz., Anteil ,Chondrit, HW-Zeit, Wärmeproduktion[W/kg]
   A = [    3.2 , 0.0073 ,    0.02 ,   0.70  , 5.75*10^-4,235,4.40  ;   % U238
            3.2 , 0.9927 ,    0.02 ,   4.47  , 9.17*10^-5,238,4.27  ;   % U235
               11.0 , 1      ,    0.08 , 14.00  , 2.56*10^-5,232,4.08 ;   % Th
         24100.0 , 0.00012, 240.00 ,   1.28  , 3.48*10^-9,  40,1.35 ];   % K40
faraday = 96485;
A(:,5) = A(:,7)*(log(2))*faraday./A(:,6)./(A(:,4)*Ga2s)*10^9;
A(:,3) = A(:,3)*ppm;
if t==0
   Mcore = sum(m(1:cmb));
   Mmantle = sum(m(cmb+1:steps));
   C = zeros(4,steps);
   M = sum(m);
   for i=1:1:4
       cm(i) = A(i,2)*A(i,3)*M/Mmantle;
       C(i,cmb+1:steps) = cm(i);
       mrad(i) = cm(i)*Mmantle;
   end;
   mold = zeros(1,4);
   Hdat = [mrad,mold,cm,steps];
end;

if t>0
if Hdat(13)-bot>=2
   mrad = Hdat(1:4);
   mold = Hdat(5:8);
   cm = Hdat(9:12);
   top = Hdat(13);
   Mmantle = sum(m(cmb+1:bot));
   Mcrust = sum(m(bot+1:top));
   for i=1:1:4
       cc(i) = cm(i)*D;
       mcrust(i) = cc(i)*Mcrust;
       mold(i) = mold(i)+mcrust(i);
       mmantle(i) = mrad(i)-mold(i);
       if mmantle(i)<0
          mmantle(i)=0;
       end;
       cm(i) = mmantle(i)/Mmantle;
       C(i,bot+1:top) = cc(i);
       C(i,cmb+1:bot) = cm(i);
   end;
   Hdat = [mrad,mold,cm,bot];
end;
end;
for i=1:1:4
   H0(i,:) = A(i,5)*C(i,:)*0.5^((t-tmax)/Ga2s/A(i,4));
end;
H = sum(H0,1);
```

mt_start.m (Function)

```
function [Tf1,Tf2,HShi,HSlo] = mt_start(steps,rx,T,cw,Tp,N)
% Function to calculate magnetometer transfer function
%-------------------------------------------------------------------
steps = 1001;
   cw = cw*10^-6;
    R = 1737000;
   rx = R-rx;
    r = linspace(R,0,steps);
   dr = r(1)-r(2);
    w = 2*pi./Tp;
  mu0 = 4*pi*10^-7;
    T = fliplr(T);
[HSlo,HShi,index] = mt_conductivity(steps,r,rx,T,cw);

for j=1:1:2
    if j==1
        s = (HShi);
    else
        s = (HSlo);
    end;
    M = sparse(steps-2,steps-2);
 for n=1:1:N
 for i=1:1:steps-2
     M(i,i) = -2/dr^2 -1i*w(n)*mu0*s(i+1)+2/r(i+1)^2;
     if i>1
   M(i,i-1) = 1/dr^2;
     end;
     if i<steps-2
   M(i,i+1) = 1/dr^2;
     end;
 end;
 B = sparse(steps-2,1);
 B(1,1) = -1/dr^2;
 G = sparse(steps,1);
 G(2:steps-1,1) = M\B;
 G(1,1) = 1;
 for i=1:1:steps
 if i==1
    gam(i) = r(1)/2*(G(2,1)-G(1,1))/dr;
 end;
 if i>1 && i<steps
    gam(i) = r(1)/2*(G(i+1,1)-G(i-1,1))/(2*dr);
 end;
 if i==1
    gam(i) = r(1)/2*(G(steps,1)-G(steps-1,1))/dr;
 end;
 end;
 rhoa(n) = w(n)*mu0*r(1)^2/(4*(abs(gam(2)))^2);
 end;
if j==1
   Tf1 = rhoa;
else
   Tf2 = rhoa;
end;
end;
```

mt_conductivity.m (Function)

```
function [HSlo,HShi,index] = mt_conductivity(steps,r,rx,T2,cw)
% Function link electrical conductivity to mineralogy
%-----------------------------------------------------------------
Rc = 8.3145/1000;
 k = 8.617e-5;
 R = 1737000;
r2 = linspace(R,0,size(T2,2));
 T = interp1(r2,T2,r);              % interpolate T
for i=1:1:steps
     sol(i) = 10.^2.4*exp(-154/(Rc*T(i)))+10.^3.1*(cw.^0.62)*exp(-87/(Rc*T(i)));
    sopx(i) = 10.^2.4*exp(-147/(Rc*T(i)))+10.^2.6*(cw.^0.62)*exp(-82/(Rc*T(i)));
    scpx(i) = 10.^3.8*exp(-1.73/(k*T(i)));
     sgt(i) = 10.^2.5*exp(-128/(Rc*T(i)))+10.^2.9*(cw.^0.63)*exp(-70/(Rc*T(i)));
    shyp(i) = 120.3*exp(-0.18./(k*T(i)));
    stro(i) = 0.35*exp(-0.79./(k*T(i)));
    sano(i) = 507.76*exp(-1.39./(k*T(i)));
    shyp = stro;
end;
M = load('sel_min.txt');
M = M/100;
for i=steps:-1:1
    if r(i)<=rx(3)
        HShi(i) = 100;
        HSlo(i)= 100;
        index(1) = i;
    end;
    if r(i)>rx(3) && r(i)<=rx(2)       q = 3;
        HShi(i) = 1/(M(q,1)/(sol(i)+2*sgt(i))+M(q,4)/(sgt(i)+2*sgt(i))+M(q,12)/(sopx(i)+2*sgt(i))+...
        ...M(q,16)/(scpx(i)+2*sgt(i)))-2*sgt(i);
        HSlo(i)= 1/(M(q,1)/(sol(i)+2*scpx(i))+M(q,4)/(sgt(i)+2*scpx(i))+M(q,12)/(sopx(i)+2*scpx(i))+...
        ...M(q,16)/(scpx(i)+2*scpx(i)))-2*scpx(i);
        index(2) = i;
    end;
    if r(i)>rx(2) && r(i)<=rx(1)-(R-rx(1))/2   q = 2;
        HShi(i) = 1/(M(q,1)/(sol(i)+2*sgt(i))+M(q,4)/(sgt(i)+2*sgt(i))+M(q,12)/(sopx(i)+2*sgt(i))+...
        ...M(q,16)/(scpx(i)+2*sgt(i)))-2*sgt(i);
        HSlo(i)= 1/(M(q,1)/(sol(i)+2*scpx(i))+M(q,4)/(sgt(i)+2*scpx(i))+M(q,12)/(sopx(i)+2*scpx(i))+...
        ...M(q,16)/(scpx(i)+2*scpx(i)))-2*scpx(i);
        index(3) = i;
    end;
    if r(i)>rx(1)-(R-rx(1))/2 && r(i)<=rx(1)   q = 1;
        HShi(i) = 1/(M(q,1)/(sol(i)+2*stro(i))+M(q,4)/(sano(i)+2*stro(i))+M(q,12)/(stro(i)+2*stro(i))+...
        ...M(q,16)/(scpx(i)+2*stro(i)))-2*stro(i);
        HSlo(i)= 1/(M(q,1)/(sol(i)+2*sano(i))+M(q,4)/(sano(i)+2*sano(i))+M(q,12)/(stro(i)+2*sano(i))+...
        ...M(q,16)/(scpx(i)+2*sano(i)))-2*sano(i);
        index(4) = i;
    end;
    if r(i)>rx(1)       q = 1;
        HShi(i) = 1/(M(q,1)/(sol(i)+2*shyp(i))+M(q,4)/(sano(i)+2*shyp(i))+M(q,12)/(shyp(i)+2*shyp(i))+...
        ...M(q,16)/(scpx(i)+2*shyp(i)))-2*shyp(i);
        HSlo(i)= 1/(M(q,1)/(sol(i)+2*sano(i))+M(q,4)/(sano(i)+2*sano(i))+M(q,12)/(shyp(i)+2*sano(i))+...
        ...M(q,16)/(scpx(i)+2*sano(i)))-2*sano(i);
    end;
end;
```

tid_start.m (Function)

```
function [k2,Q] = tid_start(steps,R,r,T,P,g,Ghl,VARc,cw,f)
% Function to calculate k2 and Q-factor
%--------------------------------------------------------------
     G = sum(Ghl,1)/2;
     V = 4/3*pi*R^3;
  rho0 = VARc(1)/V;
   eta = tid_visc(P,T,cw);
etaliq = 5*10^16;
   eta = ((1./eta.*(1-f))+(1./etaliq*f)).^-1;
for i=1:1:VARc(5)-1
        if f(i)==0
        eta(i) = 10^18;
        else
        eta(i) = 10^-3;
        end;
end;
        w = 2*pi/(3600*24*365);
G_complex = 1i*w*G./(1i*w+G./eta);
        s = r/R;
       ds = s(2)-s(1);
    Gmean = 0;
for i=1:1:steps
    Gmean = Gmean+3*G_complex(i)*s(i)^2*ds;
end;
     Gbar = (19/2*Gmean/(rho0*R*g(steps)));
       k2 = 1.5/(1+Gbar);
        Q = log10(abs(abs(k2)/imag(k2)));
       k2 = abs(k2);
```

tid_visc.m (Function)

```
function eta = tid_visc(P,T,cw)
% Function to calculate viscosity for maxwell-relaxation
%--------------------------------------------------------------
  e = 10^-16;
  A = 90;
  H = 480000;
  V = 11*10^-6;
  n = 3.5;
  r = 1.2;
coh = 16.2*cw;
  R = 8.3145;
eta = e^((1-n)/n)*A^(-1/n)*coh^(-r/n)*(exp(-(H+P*V)./(R*T))).^(-1/n)*10^6;
```

Appendix B – Parameter values

Thermal expansivity α, shear- and bulk-modulus (G and K) and their temperature and pressure derivatives for different minerals.

Phase	α [10^{-5} K^{-1}]	K_0 [GPa]	dK/dP	dK/dT [GPa/K]	G_0 [GPa]	dG/dP	dG/dT [GPa/K]
Olivin	3.1	129	5.1	0.016	82	1.8	0.013
Clino-Pyroxene	3.2	104	5.0	0.012	77	2.0	0.012
Ortho-Pyroxene	2.7	113	4.5	0.013	67	1.7	0.010
Anorthite	4.9	80	5.0	0.020	45	1.6	0.012
Spinell	2.4	174	4.9	0.019	114	1.8	0.014
Garnet	2.8	175	4.9	0.019	95	1.6	0.013
Titanite	2.5	120	5.0	0.010	70	1.5	0.010

Table 8: *Elastic moduli and their derivatives were taken from Duffy & Anderson (1989). Values for thermal expansivity stems from Robertson (1988).*

Chondritic concentration of elements [X], fraction of isotope x, decay energy E_{decay} and half-life period τ of radioactive isotopes.

Isotope	$[X]_{chondrit}$ [ppm]	x	E_{decay} [MeV]	τ [Ga]
U-238	0.02	0.9927	4.27	4.47
U-235	0.02	0.0073	4.40	0.70
Th-232	0.08	1	4.00	14.00
K-40	240	0.00012	1.35	1.28

Table 9

Parameters for the electrical conductivity calculation of minerals.

Phase	σ_0 [S/m]	E_A	σ_{cw} [S/m]	E_{cw} [kJ/mol]	r_{cw}	Source
Olivin	251.2	154 kJ/mol	1258.9	87	0.62	Dai & Karato (2009)
Ortho-Pyroxene	249.3	147 kJ/mol	398.1	82	0.62	Dai & Karato (2009)
Garnet	316.2	128 kJ/mol	794.3	70	0.63	Dai & Karato (2009)
Clino-Pyroxene	6309.6	1.73 eV				Yang et al (2011)

Table 10

The mineralogical composition of the crust and the mantle provided by *Kuskov et al (2014)*.

2330

z1	z2	Ol	Fo	Fa	Al-pha	Plag	AFS	Gross	Pyr	Alm	AlSp	FeSp
0	50	0	0	0	50	0,95	0,05	0	0	0	0	0
50	100	11,73	0,84	0,16	1,92	0	0	0	0	0	0,6	0,4
100	200	12	0,84	0,16	1,65	0	0	0	0	0	0,63	0,37
200	300	12,6	0,84	0,16	1,47	0	0	0	0	0	0,65	0,36
300	400	14	0,85	0,15	0,88	0	0	0,08	0,6	0,32	0	0
400	500	14,03	0,85	0,15	0,92	0	0	0,05	0,7	0,25	0	0
500	750	54,05	0,92	0,08	4,18	0	0	0,04	0,8	0,16	0	0
750	1000	54,67	0,91	0,09	4,61	0	0	0,04	0,8	0,16	0	0
1000	1387	54,42	0,91	0,09	4,43	0	0	0,04	0,8	0,16	0	0
z1	z2	Opx	Enst	Diop	Ferro	Cpx	Enst	Diop	Ferro	Hede	Tit	Ilm	Gei
0	50	49,6	0,85	0	0,15	0	0	0	0	0	0,4	0,88	0,13
50	100	77,06	0,84	0	0,16	8,87	0,12	0,44	0,31	0,13	0,42	0,88	0,13
100	200	76,45	0,83	0	0,17	9,45	0,18	0,53	0,1	0,2	0,45	0,84	0,16
200	300	76,45	0,82	0,02	0,16	9,47	0,24	0,44	0,1	0,22	0,42	0,76	0,24
300	400	76,29	0,8	0,05	0,15	8,39	0,3	0,4	0,1	0,2	0,43	0,68	0,32
400	500	78,9	0,78	0,04	0,18	5,72	0,33	0,33	0,14	0,2	0,43	0,56	0,44
500	750	4,3	0,85	0,05	0,1	37,1	0,36	0,32	0,1	0,22	0,37	0,4	0,6
750	1000	1,76	0,85	0,05	0,1	38,59	0,39	0,32	0,1	0,19	0,38	0,35	0,65
1000	1387	0	0	0	0	40,78	0,42	0,3	0,1	0,18	0,38	0,28	0,72

Table 11: *Mineralogical composition. Depth location boundaries z1 and z2 are given in km. Solid colored values are in %. Light colored values are fractions of the individual minerals composition.*